

รายงานการวิจัยสรุปโครงการ

เรื่อง

การศึกษาการเปลี่ยนแปลงโปรตีนในเซลท่อไตส่วนปลายในภาวะเบาจืดจาก แคลเซียมในเลือดสูง

โดย

รองศาสตราจารย์ แพทย์หญิงสุขเกษม โฆษิตเศรษฐ

ผู้ช่วยศาสตราจารย์ นายแพทย์ ดร. ปณภัฏ เอื้อวิทยา

ดร. สิทธิรักษ์ รอยตระกูล

ธันวาคม 2555

รายงานการวิจัยสรุปโครงการ

เรื่อง

การศึกษาการเปลี่ยนแปลงโปรตีนในเซลท่อไตส่วนปลายในภาวะเบาจืดจาก แคลเซียมในเลือดสูง

โดย

รองศาสตราจารย์ แพทย์หญิงสุขเกษม โฆษิตเศรษฐ

ผู้ช่วยศาสตราจารย์ นายแพทย์ ดร. ปณภัฏ เอื้อวิทยา

ดร. สิทธิรักษ์ รอยตระกูล

ธันวาคม 2555

สนันสนุนโดยสำนักงานกองทุนสนับสนุนการวิจัย

บทคัดย่อ

รหัสโครงการ: RMU5380032

ชื่อโครงการ: การศึกษาการเปลี่ยนแปลงโปรตีนในเซลท่อไตส่วนปลายในภาวะเบาจืดจาก แคลเซียมใน เลือดสูง

ชื่อนักวิจัยร่วม และสถาบัน

1. รศ. พญ.สุขเกษม โฆษิตเศรษฐ

สาขาวิชากุมารเวชศาสตร์ คณะแพทยศาสตร์ มหาวิทยาลัยธรรมศาสตร์

2. ผศ. นายแพทย์ ดร. ปณภัฏ เอื้อวิทยา

ภาควิชาสรีรวิทยา คณะแพทยศาสตร์ศีริราชพยาบาล มหาวิทยาลัยมหิดล

3. ดร. สิทธิรักษ์ รอยตระกูล

ศูนย์วิจัยพันธุ์วิศวกรรมและเทคโนโลยีชีวภาพแห่งชาติ สวทช กระทรวงวิทยาศาสตร์

ระยะเวลาโครงการ: 1 กรกฎาคม 2553 ถึง 31 มิถุนายน 2555

คำหลัก: ภาวะเบาจืด แคลเซียมในเลือดสูง

วัตถุประสงค์ของโครงการ

เพื่อศึกษาโปรตีนที่เกิดการเปลี่ยนแปลงในเซลส์ท่อไตในภาวะเบาจืดจากระดับแคลเซียมในเลือดสูง

ผลงานจากโครงการวิจัย

- 1. การเสนอผลงานในที่ประชุมวิชาการระดับนานาชาติ 3 เรื่อง
 - 1.1 เรื่อง Quantitative phosphoproteomics of hypercalcemia induced nephrogenic diabetes insipidus ที่ประชุม the Experimental Biology 2012 Annual Meeting April 21-25, 2012 in San Diego, California, USA ตามเอกสารแนบที่ 1.
 - 1.2 เรื่อง Quantitative phosphoproteomics of bilateral ureteral obstruction induced nephrogenic diabetes insipidus ที่ประชุม The American Society of Nephrology kidney week annual meeting 2011, Philadelphia, USA ตามเอกสารแนบที่ 2.
 - 1.3 เรื่อง Quantitative proteomics of hypokalemia induced nephrogenic diabetes insipidus ที่ประชุม the Experimental Biology 2013 Annual Meeting April 20-24, 2013 in Boston, Massachusetts, USA ตามเอกสารแนบที่ 3
- ผลงานตีพิมพ์แล้วในวารสารนานาชาติ 1 เรื่อง
 Tropical distal renal tubular acidosis: clinical and epidemiological studies in 78 patients
 Q J Med 2012; 105:861–877 ในฐานข้อมูล Pubmed ตามเอกสารแนบที่ 4
- 3. ผลงานที่อยู่ในขั้นตอนการส่งตีพิมพ์ในวารสารระดับนานาชาติ 2 เรื่อง จะขอส่งให้เมื่อ ได้รับการตีพิมพ์แล้ว
 - 3.1 Proteomics and Phosphoproteomics Profiling Reveal Involvement of Intergrin
 Signaling Pathway and Actin Cytoskeletal Organization in Hypercalcemia-induced
 Nephrogenic Diabetes Insipidus ตามเอกสารแนบที่ 5
 - 3.2 Proteomics Profiling Reveal Involvement of Adherens Junction and Actin cytoskeletal organization in Hypokalemia-induced Nephrogenic Diabetes Insipidus ตามเอกสารแนบที่ 6

Abstract

Nephrogenic diabetes insipidus (NDI) can be caused by hypercalcemia. The effect of early onset NDI in parathyroid hormone (PTH)-induced hypercalcemia was studied using proteomics and phosphoproteomics profiling of rat kidney medulllary collecting duct (IMCD). Tryptic peptides and phosphopeptides were identified and quantified by mass spectrometry using a label-free methodology. A total of 5,866 peptides corresponding to 1,107 proteins and 1,388 phosphopeptides of 580 proteins were identified, with significant changes in abundance of 69 proteins and 49 phosphopeptides in early onset NDI. Gene Ontology terms and pathway analysis revealed that hypercalcemia-affected proteins and phosphoproteins are from integrin signaling pathway and actin cytoskeleton organization. Immunoblotting revealed altered abundances of vasopressin-regulated phosphorylation of aquaporin-2 (Aqp2) at Ser256 and Ser261, and decreased abundance of urea transporter UT-A1 (Slc14a2) and UT-A3, together with their phosphorylation at Ser486. This is the first report of the involvement of integrin signaling pathway in urine concentration mechanism in hypercalcemia-induced early onset NDI.

Introduction

Hypercalemia, a high serum calcium concentration, is a life threatening condition and has potentially serious adverse effects. The main cause of hypercalcemia is excessive bone resorption induced by neoplastic processes. Tumors of the breast, lung and kidney are also the most common causes of hypercalcemia. Primary hyperparathyroidism is a common endocrine disorder causing hypercalcemia. The most common renal manifestations of hypercalcemia are polyuria and impaired urine concentrating ability, or nephrogenic diabetes insipidus (NDI). The urine concentrating defect of hypercalcemia is related to the decreased medullary tonicity by the reduced expression of bumetanide-sensitive Na-K-2Cl cotransporter (NKCC2) and the reduced responsiveness of the collecting duct to vasopressin resulting in down-regulation of aquaporin (AQP)-2 and -3 in collecting ducts as demonstrated in vitamin D-induced (1) and parathyroid hormone induced hypercalcemic rats (2, 3). However, little is known about the underlying cellular mechanism and signaling pathways affecting these processes.

Proteomic study using liquid chromatography tandem mass spectrometry (LC-MS/MS) has been proved to be powerful in global discovery of proteins involved in defined perturbation of cell condition, which is in contrast to the traditional way of "one-by-one" protein study. Thus, the purpose of this study aimed to employ this state-of-the art technology coupled with pathway analysis to identify proteins and signaling pathways involved in parathyroid hormone-induced hypercalcemia and NDI.

The present data demonstrated the earliest onset of down-regulation of AQP2 protein expression in inner medullary collecting duct in rat with hypercalcemia induced nephrogenic diabetes insipidus. The authors will apply the knowledge of the present data to study proteins involved in hypercalcemic induced nephrogenic DI by the mean of proteomic tools.

Materials and Methods:

Experimental Animals. Each study was performed in 14 males Spraque Drawleys rats, initially weighing 180-200 g. The animals were housed individually in rat metabolic cages and maintained on standard rat chow (SWT, Samutprakarn,Thailand) 3 days before starting experiments. After a period of acclimation, the animals were randomized into two groups including control rats (C, n=7) and PTH treated rats (PTH, n=7). The osmotic minipumps (Alzet 1003D, DURECT, Cupertino, CA) filled with 15ug/kg/day of PTH (1-34) (Bachem, USA) dissolved in 2% cysteine HCL, pH 2, were implanted into the subcutaneous tissue in the back area under subcutaneous tissue of PTH rats. The osmotic pumps for control rats were infused with vehicle alone. The pumps were equilibrated in normal saline for 12 h at 37°c before implantation. Rats were given free access to tab water throughout the experiments and kept in environment with a 12-h artificial light/dark cycle and a temperature of 21± 2 °c, and humidity of 55 ± 2%. The animals were euthanized by guillotine at 1, 1.5, and 2 days later.

Clearance studies. Urine collection was made under 1.5 ml of mineral oil. Body weight, water intake, 24-hr urine volume, urine osmolality were measured at the beginning of each experiment and the end point. During euthanization, thrunk blood was obtained for serum calcium, concentration. Urine calcium, and creatinine concentration were measured. Urine osmolality was measured by osmometer (Osmomat 030, Gonotec Gmb, Berlin, Germany). Urine calcium/creatinine ratio were calculated. Kidneys were harvested and inner medullas were dissected.

Sample preparation. IMCD was prepared from rats inner medullas using the method of Stroke (4) with modifications (5). Briefly, Kidney inner medullas were digested into suspension by incubation at 37°c for 70-90 min in digestion solutions (4). The IMCD suspension was subjected to three low-speed centrifugations (at 70 g, 30 s) to separate the

IMCD-enriched pellet from non-IMCD fraction in the supernatant. The IMCD pellets were subjected to centrifugation at >10,000 g for 5 min, then were lyzed in 150 ul of lysis buffer containing 8M urea/50mM Tris-HCl/75 mM NaCl with 1x protease and phosphatase inhibitor (Pierce, Rockford, IL). Protein samples were sonicated for 2 min with 0.5 sec pulse on ice. Samples were spun at 14,000 g for 10 min to pellet debris and the supernatant was saved. Protein concentration of samples was analyzed by the BCA method (Pierce, Rockford, IL). Each sample was divided into 2 portions, 100 ug and 300 ug of proteins, for phosphopeptide preparation and total peptide preparation, respectively. In-solution-trypsin digestion and ingel trypsin digestion were employed for phosphopeptide enrichment, and total peptide preparation, respectively. The sample preparation process was repeated two additional times on separate days to produce a total of four biological replicates.

Total peptide preparation: The second portion (100 ug) of each IMCD sample was subjected to one-dimensional SDS-PAGE and digested as previously described (6). Briefly, the sample was solubilized with ¼ part of Laemmli buffer and 40 mM DTT, followed by heating at 60°c for 15 min. One-dimensional SDS-PAGE was performed using a 12.5% gradient polyacrylamide gel. The protein in gel was visualized by colloidal coommassie blue staining and destaining in deionized H₂O. The gels were sliced into small pieces, destained and dehydrated by incubation in 25 mM NH₄HCO₃/50% acetronitrile (CAN) followed by drying in *vacuo*. The protein in gels was reduced with 10mM DTT for 1 h at 37°c, alkylated with 40 mM iodoacetamide for 1 h at room temperature in the dark. The gel pieces was washed with 25 mM NH₄HCO₃ once followed by washing with 25 mM NH₄HCO₃/50% acetronitrile twice, and then dried in *vacuo*. The dried gel pieces were immersed in 25 mM NH₄HCO₃ containing 12.5 ng/µl trypsin at 37°c overnight. The tryptic peptides were extracted with 50% ACN/0.1%FA and sonication in a water bath for 20 min. This step was

repeated thrice. The samples were dried in *vacuo* and reconstituted with 10 ul of 0.1% formic acid for LC-MS/MS analysis.

Phosphopeptide preparation: The second portion (300 ug) of each IMCD sample was reduced with 10mM DTT for 1 h at 37°c, alkylated with 40 mM iodoacetamide for 1 h at room temperature in the dark, and then quenched with 40mM DTT for 15 min. Samples were diluted with 50mM ammonium bicarbonate buffer to < 1M urea, followed by digestion with trypsin overnight at 37°c using an enzyme-to-protein ratio 1:22 to 1:30 (wt:wt). Samples were then acidified with 0.5% formic acid and were desalted on a 1 cc Oasis HLB cartridge (Waters, Milford, MA). Phosphopeptides was enriched by Ga³⁺- NTA phosphopeptide enrichment kit (IMAC) (Thermo Scientific).

LC-MS/MS Analysis The dried samples were reconstituted in 10 μL of the buffer consisted of 0.2% formic acid in de-ionized water and analyzed by LTQ Orbitrap XL mass spectrometry (Thermo Fisher Scientific, San Jose, CA, USA) equipped with a nanoflow Ultra-high Pressure Liquid Chromatography system (nanoACQUITY UPLC, Waters Corp., Milford, MA, USA). A total of 8 μL sample was loaded onto a C18 trap column (5 μm, 180 μm X 20 mm, Waters), followed by separation using a C18 column (75 μm × 25-cm,1.7-μm, ACQUITY UPLC BEH130 C18, Waters). Buffer A was 0.1% formic acid in de-ionized water, and buffer B was 0.1% formic acid in acetonitrile. A linear gradient from 3% to 35% B over a 90-min period at a flow rate of 350 nL/min was applied. The peptides were analyzed in the positive ion mode by electrospray ionization (spray voltage = 1.8 kV). The MS was operated in a data-dependent mode, in which one full scan with m/z 300-2000 in the Orbitrap (R=60000 at m/z 400) using a rate of 30 ms/scan. The five most intense peaks for fragmentation with a normalized collision energy value of 35% in the LTQ were selected. A repeat duration of 30 s was applied to exclude the same m/z ions from the re-selection for fragmentation.

Database Searching The mass spectra were searched using two different search algorithms, SEQUEST(7), and InsPecT(8). Searches were performed against the most recent rat RefSeq database (NCBI) which included a list of common contaminating proteomes from other species. All datasets were filtered for a FDR of <1% estimated based on target-decoy analysis(9). Label free peptide quantification was performed using QUOIL software(10). Phosphorylation site performed localization was using PhosSA software(11). Phosphopeptides matching to multiple protein isoforms were identified using ProMatch software (12). Gene Ontology (GO) was performed using software provided by Dr. Mark A. Knepper (NHLBI, NIH, USA).

Bioinformatics *The* DAVID bioinformatic tool (http://david.abcc.ncifcrf.gov/)(13) was used to identify certain classes of proteins based on GO terms, the list of the KEGG (http://www.genome.jp/kegg/pathway.html) and PANTHER pathway terms (www.pantherdb.org/pathway). String database (http://string-db.org) was used to create a functional associate protein networks (14).

Immunoblotting and antibodies. Dissected inner medullas were homogenized in sucrose solutions (250 mM sucrose, 10 mM triethanolamine, pH 7.6) with five strokes of a motor-driven Potter-Elvehjem homogenizer at 2,500 rpm. The quantity of protein was determined spectrophotometrically on all samples in a single assay (Pierce BCA protein assay kit, Thermoscientific, IL, USA). These samples were solubilized in Laemmli sample buffer containing 7.5% sodium dodecyl sulfate (SDS)(15).

After solubilization, protein samples (7ug) were loaded on to SDS-page gel electrophoresis on 12% polyarylamide gels then stained with Coomassie brilliant blue. The concentrations of each protein sample were normalized based on the results of coommassie brilliant blue staining gels. Protein samples (10 ug) were resolved by SDS-page gel

electrophoresis on 12% polyarylamide gels and transferred electrophoretically onto nitrocellulose membranes. The membranes were then blocked for 1 h with 5% non fat milk with TTBS (20mM Tris, 150mM NaCl, 0.05% Tween 20 pH 7.5), rinsed and probed with primary antibodies overnight at 4°c. Anti AQP2 antibody (5007)(16), anti pS256 AQP2 (17), anti pS261 AQP2(18), anti pS269 AQP2(16), anti UT-A1 (L194) (19), anti UT-A3 (Q2695)(20), anti pS84-UT-A1/3 (P7282) (21), anti pS486-UT-A1 (P7284) (21) were kindly gifted by Dr. Mark A. Knepper (NIH, USA). Other antibodies including Myh10 (3403), Cortactin (3502), ERM (3142), Pxn (2542), Fak (3285), Vlc (4650), and Igb1 (4706) were purchased from cell signaling technology (MA, USA).

The blots were washed with TTBS (3 x 5min) and incubated with horseradish peroxidase-conjugated goat anti-rabbit IgG 1 h (Thermoscientific, IL, USA) followed by washing with TTBS (3 x 10 min). Antibody binding was visualized using supersignal west pico chemiluminescent substrate (Thermo scientific, IL, USA). Chemiluminescent was imaged and quantified by ChemiDoc XRS (Biorad, CA, USA).

Statistical analysis. Results are express as means \pm SE. Statistical significance between experimental groups was determined by Student's T-test, and P < 0.05 was considered significant.

RESULTS

Effect of PTH on Serum Ca, urine output, urine osmolality, and urine calcium.

Rats treated with PTH developed significant hypercalcemia as compared with control rats on day 1. (serum Ca $9.3\pm0.4~vs$. $8.8\pm0.3~mEq/L$, P=0.05, fig. 1). This was persistent until 2 days of experiment. The PTH rats produced significantly more urine than controls on day1 (0.08 $\pm0.006~vs$. 0.11 ± 0.005 ml/100g/hr, P<0.05, fig. 3). Urine osmolality of PTH rats were significantly lower than those of controls on day 1 (1.84 \pm 0.1 vs. 1.38 ± 0.1 osmol/kgH₂O, P<0.05, fig. 2). PTH rats significantly excreted urine calcium/creatinine more than controls on day 1 (0.29 $\pm0.04~vs$. 0.55 ± 0.06 mg/mg, P<0.01, fig.4.) PTH rats had significant lower body weight than controls on 2 days ($212\pm3.9~vs$. 220 ± 4 gram, P<0.05, fig. 5).

Effect of PTH on Ca and P clearance

To assess effect of PTH on renal tubular function, we studied renal clearance of Ca, P, Na and K at different time points. Urine calcium to creatinine ratio of PTH rats significantly increased as early as 1 day accompanied with significant hypercalcemin on the 1st days (figure 6). Serum P and tubular reabsorption of P on PTH rats were not different from those of controls on day 1-2 as shown on figure 7 and 8, respectively.

Effect of PTH on Na and K clearance

Serum Na of rats treated with 15ug/kg/day of PTH significantly lower than those of controls on Day 2 (133.4±1.4 vs. 135.1±1.5, *P*<0.05, figure 9). Rats treated with PTH excreted more Na in urine than controls on day 1.5 and 2 as demonstrated in fractional excretion of Na (figure 10). However, these didn't reach significant difference.

Proteomics and phosphoproteomics profiling, quantification and bioinformatics analysis

Rats were treated with PTH or vehicle for 1 day, and IMCD was isolated by enzyme digestion, followed by digestion with trypsin. Four replicates were analyzed by LTQ-Orbitrap MS. A total of 6,161 peptides passed the target-decoy criteria with a false discovery rate (FDR) < 1% for single peptides. Analysis of dataset using two search algorithms, InsPecT and SEQUEST, revealed 3,489 and 4,320 peptides, respectively (Fig. 14A). Promatch program was employed to identify 5,866 unambiguous peptides, corresponding to 1,107 proteins. The areas under the MS1-time course chromatograms from the unambiguous peptides were quantified using Qouil software. A histogram of the ratios of quantified peptides showed that the majority of peptides did not change substantially between hypercalcemic and control IMCDs (Fig. 14B). Table 1 and 2 demonstrated a set of 57 decreased and 11 increased proteins whose ratios met the dual criteria, $|\log_2[PTH/control]|$ of 0.58 and two tailed t-test against $\log_2(1)$ of P < 0.05. The complete list of proteins identified and their GO terms can be found in.

We employed the David bioinformatics tool to identify the classes of proteins, and database search genomes (KEGG) to reveal the identities over- and under-represented proteins among the proteins affected by induction of hypercalcemia. GO molecular function terms that are significantly changed are proteins with GO *biological processes* and *molecular functions* terms "generation of metabolite and energy", "cytoskeleton and protein binding" and "regulation of actin cytoskeleton organization" (Fig. 15A). The KEGG pathways that are significantly changed include "ECM-receptor interaction", and "regulation of actin cytoskeleton organization". A number of proteins involved in vesicle trafficking, microtubule motor activity and Aqp2 trafficking were identified (Fig. 16A).

We enriched phosphopeptides of IMCD using IMAC (Fig. 13B), which then were identified by LC-MS/MS. A total of 1,601 phosphopeptide scans passed the target-decoy criterion with FDR < 1% for single phosphopeptides. PhosSA program was used to assign 1,195 phosphorylation sites as being from 577 proteins. The 156 phosphopeptides of 143 proteins identified in at least three independent experiments were quantified and a histogram of [log₂PTH/Control] ratios of quantified phosphopeptides are shown in Fig. 14D, and their GO terms and kinase motifs are shown in. The 49 phosphopeptide ratios meeting the dual criteria are listed in Table 3.

Among the phosphoproteins that differed in amounts from control samples, the molecular function GO terms that are significantly changed include proteins with GO biological processes and molecular functions terms "cytoskeletal protein binding" and "regulation of cytoskeleton organization" (Fig. 15B) and KEGG pathway "regulation of actin cytoskeleton".

When the combined lists of phosphoproteins and total proteins identified as described above were analyzed, the biological GO term "regulation of actin cytoskeleon" emerged as expected (Fig. 15C). KEGG and PANTHER pathways significantly enriched among the 118 affected proteins and phosphoproteins were ECM-mediated focal adhesion and integrin signaling pathway (Fig. 15D, 15E). Most of the phosphorylation sites regulated by hypercalcemia have been previously identified in IMCD in response to vasopressin(22, 23). Other down-regulated phosphoproteins involved in vesicle trafficking, microtubule motor activity are shown in Fig. 16B. The kinase motifs among the affected phosphopeptides were identified by KinaseMotif classifier program (NHLBI, NIH), with proline-directed motifs identified in 50% of phosphopeptides decreased in hypercalcemia.

Effects of hypercalcemia/hypercalciuria on actin cytoskeletal organization.

The down expression of actin cytoskeletal organization in hypercalcemia was confirmed by immunoblotting. Consistent with the proteomics profiling, there are significant down-regulation of Cttn and ERM (but not of Myh10) were demonstrated (Fig. 17).

Effects of hypercalcemia/hypercalciuria on ECM-mediated focal adhesion and integrin signaling pathway.

Down regulation of ECM-mediated focal adhesion and integrin signaling pathway in hypercalcemia was confirmed by multiple reaction monitoring (MRM) with a list of peptides identified.

Effects of hypercalcemia/hypercalciuria on vasopressin-sensitive phosphorylation sites of Aqp2 and UT-A1/3

Phosphoproteomics profiling showed a down-regulation of vasopressin-sensitive phosphorylation site of Aqp2 (Ser256), but not of total Aqp2 in response to hypercalcemia (Suppl.Fig.1), which was confirmed by immunoblotting, but the abundance of pSer261 is significantly up-regulated (Fig. 18). Although MS did not show significant change in Slc14a2 (urea transporter 2 isoform 1) level, immunoblotting demonstrated significant down-regulation of UT-A1, pS486 of UT-A1 and UT-A3 levels (Fig. 18).

Effects of hypercalcemia/hypercalciuria on serum vasopressin and on cAMP levels in whole inner medulla (IM).

Levels of serum vasopressin and IM cAMP, determined by ELISA, are not different between PTH-induced hypercalcemia/hypercalciuria and control rats (Fig.19).

DISCUSSION

We report for the first time the use of proteomics and phosphoproteomics to identify and quantify changes in rat renal IMCD proteins and phosphoproteins resulting from PTH-induced hypercalcemia/hypercalciuria. From a total of 5,866 unambiguous tryptic peptides corresponding to 1,107 proteins, 439 proteins were identified in at least three experiments, of which 69 (15%) proteins are significantly changed in abundance in hypercalcemia/hypercalciuria rats. As for phosphoproteins, a total of 1195 unambiguous phosphorylation sites in 577 proteins were identified, of which 49 phosphorylation sites are significantly changed in abundance in hyper-calcemia/hypercalciuria IMCD. In this study, we discovered new 217 phosphorylation sites of 111 proteins according to latest data of phosphositeplus (www.phosphosite.org)(24).

According to our findings, we can draw the following conclusions: (i) affected proteins and phosphoproteins of rat IMCD are predominantly those with GO terms "cytoskeleton and protein binding" and "regulation of actin cytoskeleton organization"; (ii) hypercalcemia/hypercalciuria affects ECM-mediated focal adhesion and integrin signaling pathway (iii) phosphorylation of Aqp2-Ser256 is decreased but -Ser261 increased in hypercalcemia/hypercalciuria; (iv) total UT-A1, including phospho(Ser486)-UT-A1, and total UT-A3 contents are decreased in hypercalcemia/hypercalciuria; (v) IM cAMP and serum vasopressin levels are not changed in early NDI.

Water permeability of collecting duct is controlled by AVP which stimulates translocation of Aqp2 from intracellular vesicles to plasma membrane. Actin involves in Aqp2 exocytosis by providing a tract for Aqp2 containing vesicle trafficking to plasma membrane(25). High extracellular Ca²⁺ increases F-actin content preventing Aqp2 translocation to the plasma membrane(26). Consistent with previous findings, we found that

hypercalcemia regulated proteins and phosphoproteins involved in F-actin polymerization e.g. Cpgn and Rdx which cap the barbed ends of F-actin filaments, and Lasp1 which plays important role in the regulation of dynamic actin-based cytoskeletal activities. In addition, in this study, hypercalcemia also decreased ezrin-radixin-moesin, RhoA activators. Inhibition of RhoA induces depolymerization of F-actin, Aqp2 translocation to apical membrane and delays Aqp2 internalization(27, 28). Thus, hypercalcemia may lead to activation of RhoA which was directly involved in Aqp2 trafficking to plasma membrane(27).

Reorganization of microtubules was accompanied with vasopressin-induced Aqp2 translocation to apical membrane(29). Non-muscle myosin IIA (Myh9) has been implicated in Aqp2 trafficking via vasopressin-mediated activation of the Ca⁺² calmodulin pathway(30). In contrast to vasopressin regulation(22), we found that phosphorylation of Myh9 at Ser1944 was down-regulated in response to hypercalcemia. In this study, hypercalcemia decreased abundances of Arpc2 and Arpc1b, component of actin-related protein 2/3 complex which plays major role in local actin polymerization at the interface between vesicles and plasma membrane at the docking site(31). We found that, hypercalcemia also down-regulated many proteins and phosphoproteins involved in clathin-mediated endocytosis which associated in the internalization of Aqp2 by dynamin-dependent pathway(32). Particularly V-type proton ATPase subunit (Atp6v1h) which providing most of the energy required for transport processes in the vacuolar system were down-regulated by hypercalcemia in this study. Motor protein dynein has been implicated in centripetal transport of Aqp2 after internalization(29). Interestingly, we found that Dync1h1 and phosphorylation of Dync1li1, parts of dynein complex were down-regulated by hypercalcemia.

Integrin signaling directly culminates in reorganization of actin cytoskeleton, which plays an important role in Aqp2 translocation(33). We identified changes in abundances of

12 proteins involved in ECM receptor interaction, focal adhesions and integrin signaling pathway in hypercalcemia/hypercalciuria, namely, Arpc1b, Arpc2, Lamb2, Lamc1, Agrn, Itgb1, Pxn, Col4a1, Col4a3, Col6a3, Nid1, and Pak2. A number of studies have shown an association between integrin signaling pathway and Aqp2 in kidney collecting duct. For instance, mice with gene ablation of both Nid1 and Nid2 (nidogen-1 and -2) manifest hydronephrosis(34); and those with inactivated Lamc1(laminin gamma-1) or inactivated Itgb1 (integrin beta-1) have reduced levels of vasopressin receptor and Aqp2 expression resulting in NDI^{20,21}. In IMCD, integrin β 1 present in Aqp2-containing vesicles directly binds to Aqp2 at integrin-binding motif and modulates Aqp2 trafficking(35)'(36) and promotes epithelial morphogenesis(37).

In IMCD high extracellular [Ca²⁺] in urine stimulates calcium sensing receptor (CaSR) followed by the release of intracellular calcium(38, 39). This CaSR-mediated release of intracellular calcium is coupled to integrin β1 promotion of cellular adhesion and migration(40). Taken together, stimulation of CaSR by high [Ca²⁺] in urine may induce NDI via integrin-Aqp2 interaction or via an integrin signaling pathway and cytoskeleton reorganization.

Vasopressin regulates Aqp2 by increasing phosphorylation at Ser256, Ser264, Ser269 and decreasing phosphorylation at Ser261 located at C-terminal(22, 41-43). Phosphorylation at Ser256 is required for trafficking of Aqp2-bearing vesicles to plasma membrane(42, 44, 45), while that of phosphoSer261 is involved in polyubiquitination and proteasomal degradation(46). Decreased abundance of total Aqp2 and phosphoSer256-Aqp2 have been observed in chronic hypercalcemia induced by vitamin D for 8 days(2). Our study of early onset hypercalcemia demonstrated decreased phosphoSer256-Aqp2 and increased phosphoSer261-Aqp2 levels but without any changes in abundance of total Aqp2. Interestingly, early onset hypercalcemia did not change abundance of phosphSer269-Aqp2,

which is involved in retaining AQP2 in the plasma membrane by reducing endocytosis(47, 48). Our findings suggested that early onset hypercalcemia induces NDI due to a decrease in membrane accumulation of Aqp2 brought about by inhibition of phosphorylation at Ser256-Aqp2 and increase in phosphorylation of pSer261-Aqp2. However, the molecular mechanisms of these findings need further studies.

Vasopressin stimulates urea permeability by increasing plasma membrane levels of UT-A1 and UT-A3 accompanied by phosphorylation at Ser486 and Ser499 of UT-A1, and at Ser84 of UT-A3.(21, 49-52) Urea perfusion and transport are increased at day 14 of vitamin D-induced hypercalcemia in rat(53). On the other hand, our studies of early onset hypercalcemia show induction of NDI is accompanied by down-regulation of total abundance of UT-A1 including phosphoSer486-UT-A1 and of UT-A3 but not of phosphoSer84-UT-A3. The differences between our work and previous reports might be due to the difference in duration of hypercalcemia. Vasopressin activates PKA, which is responsible for phosphorylation of UT-A1-Ser486 and -Ser499(54), and of UT-A3-Ser84(55). Taken together, it is plausible that down-regulation of PKA might be responsible for the decrease of phosphoSer486-UT-A1 observed in hypercalcemia of early NDI.

Stimulation of CaSR modulates Aqp2 expression level by inhibiting PKA, independent of PKC and ERK(56). Activated CaSR stimulates many kinase pathways, e.g. MAPK, PKC and ERK(57). In the current study, 50% of the decrease in phosphorylation sites were of proline-directed sites. Thus, MAPK or cyclin-dependent kinase might be down-regulated in response to hypercalcemia, but the role of hypercalcemia-induced NDI on collecting duct kinases requires further investigation.

Previous studies in a rat model of vitamin D-induced NDI for 5 days demonstrated that hypercalcemia reduces cAMP level and down-regulates Aqp2 and Aqp3 abundances, which can be prevented by cAMP-phosphodiesterase inhibitor(2). However, we found no changes in cAMP level in hypercalcemia-induced early onset NDI. Proteomics analysis demonstrated almost 4-fold up-regulation of Nme2 which regulates cAMP biosynthetic process(58). Differences in cAMP levels between our findings and previous study is most likely due to difference in the duration of NDI. Early onset NDI induced by hypercalcemia may involve proteins and signaling pathways downstream of cAMP-related processes.

In summary, we report for the first time proteomics and phosphoproteomics profiling of IMCD in hypercalcemia-induced early onset NDI in a rat model. The data point to the involvement of the integrin signaling pathway and actin cytoskeletal organization in the etiology of the syndrome. In addition, hypercalcemia in early onset NDI alters vasopressin-regulated phosphorylation of IMCD Aqp2 and UT

References

- 1. Wang W, Kwon TH, Li C, Frokiaer J, Knepper MA, Nielsen S. Reduced expression of Na-K-2Cl cotransporter in medullary TAL in vitamin D-induced hypercalcemia in rats. Am J Physiol Renal Physiol. 2002;282:F34-44.
- 2. Wang W, Li C, Kwon TH, Knepper MA, Frokiaer J, Nielsen S. AQP3, p-AQP2, and AQP2 expression is reduced in polyuric rats with hypercalcemia: prevention by cAMP-PDE inhibitors. Am J Physiol Renal Physiol. 2002;283:F1313-25.
- 3. Wang W, Li C, Kwon TH, Miller RT, Knepper MA, Frokiaer J, et al. Reduced expression of renal Na+ transporters in rats with PTH-induced hypercalcemia. Am J Physiol Renal Physiol. 2004;286:F534-45.
- 4. Stokes JB, Grupp C, Kinne RK. Purification of rat papillary collecting duct cells: functional and metabolic assessment. Am J Physiol. 1987;253:F251-62.
- 5. Pisitkun T, Bieniek J, Tchapyjnikov D, Wang G, Wu WW, Shen RF, et al. High-throughput identification of IMCD proteins using LC-MS/MS. Physiol Genomics. 200;25:263-76.
- 6. Pisitkun T, Shen RF, Knepper MA. Identification and proteomic profiling of ex6osomes in human urine. Proc Natl Acad Sci U S A. 2004;101:13368-73.
- 7. Yates JR, 3rd, Eng JK, McCormack AL, Schieltz D. Method to correlate tandem mass spectra of modified peptides to amino acid sequences in the protein database. Anal Chem. 1995,15;67:1426-36.
- 8. Tanner S, Shu H, Frank A, Wang LC, Zandi E, Mumby M, et al. InsPecT: identification of posttranslationally modified peptides from tandem mass spectra. Anal Chem. 2005,15;77:4626-39.
- 9. Elias JE, Gygi SP. Target-decoy search strategy for increased confidence in large-scale protein identifications by mass spectrometry. Nat Methods. 2007;4:207-14.
- 10. Wang G, Wu WW, Zeng W, Chou CL, Shen RF. Label-free protein quantification using LC-coupled ion trap or FT mass spectrometry: Reproducibility, linearity, and application with complex proteomes. J Proteome Res. 2006;5:1214-23.
- 11. Saeed F PT, Hoffert J, Wang G, Gucek M, Knepper MA. An efficient dynamic programming algorithm for phosphorylation site assignment of large-scale mass spectrometry data. Proc of IEEE BIBM. 2012;2012.
- 12. Tchapyjnikov D, Li Y, Pisitkun T, Hoffert JD, Yu MJ, Knepper MA. Proteomic profiling of nuclei from native renal inner medullary collecting duct cells using LC-MS/MS. Physiol Genomics;40:167-83.
- 13. Huang da W, Sherman BT, Lempicki RA. Systematic and integrative analysis of large gene lists using DAVID bioinformatics resources. Nat Protoc. 2009;4:44-57.
- 14. Jensen LJ, Kuhn M, Stark M, Chaffron S, Creevey C, Muller J, et al. STRING 8--a global view on proteins and their functional interactions in 630 organisms. Nucleic Acids Res. 2009 Jan;37(Database issue):D412-6.
- 15. Marples D, Knepper MA, Christensen EI, Nielsen S. Redistribution of aquaporin-2 water channels induced by vasopressin in rat kidney inner medullary collecting duct. Am J Physiol. 1995;269:C655-64.
- 16. Hoffert JD, Fenton RA, Moeller HB, Simons B, Tchapyjnikov D, McDill BW, et al. Vasopressin-stimulated increase in phosphorylation at Ser269 potentiates plasma membrane retention of aquaporin-2. J Biol Chem. 2008;283:24617-27.
- 17. Nishimoto G, Zelenina M, Li D, Yasui M, Aperia A, Nielsen S, et al. Arginine vasopressin stimulates phosphorylation of aquaporin-2 in rat renal tissue. The American journal of physiology. 1999;276:F254-9.
- 18. Hoffert JD, Nielsen J, Yu MJ, Pisitkun T, Schleicher SM, Nielsen S, et al. Dynamics of aquaporin-2 serine-261 phosphorylation in response to short-term vasopressin treatment in collecting duct. American journal of physiology Renal physiology. 2007;292:F691-700.

- 19. Nielsen S, Terris J, Smith CP, Hediger MA, Ecelbarger CA, Knepper MA. Cellular and subcellular localization of the vasopressin- regulated urea transporter in rat kidney. Proc Natl Acad Sci U S A. 1996;28;93:5495-500.
- 20. Terris JM, Knepper MA, Wade JB. UT-A3: localization and characterization of an additional urea transporter isoform in the IMCD. Am J Physiol Renal Physiol. 2001;280:F325-32.
- 21. Hwang S, Gunaratne R, Rinschen MM, Yu MJ, Pisitkun T, Hoffert JD, et al. Vasopressin increases phosphorylation of Ser84 and Ser486 in Slc14a2 collecting duct urea transporters. Am J Physiol Renal Physiol. 2010;299:F559-67.
- 22. Hoffert JD, Pisitkun T, Wang G, Shen RF, Knepper MA. Quantitative phosphoproteomics of vasopressin-sensitive renal cells: regulation of aquaporin-2 phosphorylation at two sites. Proc Natl Acad Sci U S A. 2006;103:7159-64.
- 23. Hoffert JD, Wang G, Pisitkun T, Shen RF, Knepper MA. An automated platform for analysis of phosphoproteomic datasets: application to kidney collecting duct phosphoproteins. Journal of proteome research. [Research Support, N.I.H., Intramural]. 2007;6:3501-8.
- 24. Hornbeck PV, Kornhauser JM, Tkachev S, Zhang B, Skrzypek E, Murray B, et al. PhosphoSitePlus: a comprehensive resource for investigating the structure and function of experimentally determined post-translational modifications in man and mouse. Nucleic Acids Res. 2012;40:D261-70.
- 25. Simon H, Gao Y, Franki N, Hays RM. Vasopressin depolymerizes apical F-actin in rat inner medullary collecting duct. Am J Physiol. 1993;265:C757-62.
- 26. Procino G, Carmosino M, Tamma G, Gouraud S, Laera A, Riccardi D, et al. Extracellular calcium antagonizes forskolin-induced aquaporin 2 trafficking in collecting duct cells. Kidney Int. 2004;66:2245-55.
- 27. Tamma G, Klussmann E, Procino G, Svelto M, Rosenthal W, Valenti G. cAMP-induced AQP2 translocation is associated with RhoA inhibition through RhoA phosphorylation and interaction with RhoGDI. J Cell Sci. 2003;116:1519-25.
- 28. Tamma G, Klussmann E, Oehlke J, Krause E, Rosenthal W, Svelto M, et al. Actin remodeling requires ERM function to facilitate AQP2 apical targeting. J Cell Sci. 2005;118:3623-30.
- 29. Vossenkamper A, Nedvetsky PI, Wiesner B, Furkert J, Rosenthal W, Klussmann E. Microtubules are needed for the perinuclear positioning of aquaporin-2 after its endocytic retrieval in renal principal cells. Am J Physiol Cell Physiol. 2007;293:C1129-38.
- 30. Chou CL, Christensen BM, Frische S, Vorum H, Desai RA, Hoffert JD, et al. Non-muscle myosin II and myosin light chain kinase are downstream targets for vasopressin signaling in the renal collecting duct. J Biol Chem. 2004;279:49026-35.
- 31. Gasman S, Chasserot-Golaz S, Malacombe M, Way M, Bader MF. Regulated exocytosis in neuroendocrine cells: a role for subplasmalemmal Cdc42/N-WASP-induced actin filaments. Mol Biol Cell. 2004;15:520-31.
- 32. Sun TX, Van Hoek A, Huang Y, Bouley R, McLaughlin M, Brown D. Aquaporin-2 localization in clathrin-coated pits: inhibition of endocytosis by dominant-negative dynamin. Am J Physiol Renal Physiol. 2002;282:F998-1011.
- 33. Noda Y, Sasaki S. The role of actin remodeling in the trafficking of intracellular vesicles, transporters, and channels: focusing on aquaporin-2. Pflugers Arch. 2008;456:737-45.
- 34. Bader BL, Smyth N, Nedbal S, Miosge N, Baranowsky A, Mokkapati S, et al. Compound genetic ablation of nidogen 1 and 2 causes basement membrane defects and perinatal lethality in mice. Mol Cell Biol. 2005;25:6846-56.
- 35. Barile M, Pisitkun T, Yu MJ, Chou CL, Verbalis MJ, Shen RF, et al. Large scale protein identification in intracellular aquaporin-2 vesicles from renal inner medullary collecting duct. Mol Cell Proteomics. 2005;4:1095-106.
- 36. Tamma G, Lasorsa D, Ranieri M, Mastrofrancesco L, Valenti G, Svelto M. Integrin signaling modulates AQP2 trafficking via Arg-Gly-Asp (RGD) motif. Cell Physiol Biochem. 2011;27:739-48.

- 37. Chen Y, Rice W, Gu Z, Li J, Huang J, Brenner MB, et al. Aquaporin 2 promotes cell migration and epithelial morphogenesis. J Am Soc Nephrol. 2012;23:1506-17.
- 38. Nemeth EF, Scarpa A. Rapid mobilization of cellular Ca2+ in bovine parathyroid cells evoked by extracellular divalent cations. Evidence for a cell surface calcium receptor. J Biol Chem. 1987;262:5188-96.
- 39. Brown EM, Gamba G, Riccardi D, Lombardi M, Butters R, Kifor O, et al. Cloning and characterization of an extracellular Ca(2+)-sensing receptor from bovine parathyroid. Nature. 1993;366:575-80.
- 40. Tharmalingam S, Daulat AM, Antflick JE, Ahmed SM, Nemeth EF, Angers S, et al. Calciumsensing receptor modulates cell adhesion and migration via integrins. J Biol Chem. 2011;286:40922-33.
- 41. Christensen BM, Zelenina M, Aperia A, Nielsen S. Localization and regulation of PKA-phosphorylated AQP2 in response to V(2)-receptor agonist/antagonist treatment. Am J Physiol Renal Physiol. 2000;278:F29-42.
- 42. Fushimi K, Sasaki S, Marumo F. Phosphorylation of serine 256 is required for cAMP-dependent regulatory exocytosis of the aquaporin-2 water channel. J Biol Chem. 1997;272:14800-4.
- 43. Kamsteeg EJ, Heijnen I, van Os CH, Deen PM. The subcellular localization of an aquaporin-2 tetramer depends on the stoichiometry of phosphorylated and nonphosphorylated monomers. J Cell Biol. 2000;151:919-30.
- 44. van Balkom BW, Savelkoul PJ, Markovich D, Hofman E, Nielsen S, van der Sluijs P, et al. The role of putative phosphorylation sites in the targeting and shuttling of the aquaporin-2 water channel. J Biol Chem. 2002;277:41473-9.
- 45. Nejsum LN, Zelenina M, Aperia A, Frokiaer J, Nielsen S. Bidirectional regulation of AQP2 trafficking and recycling: involvement of AQP2-S256 phosphorylation. Am J Physiol Renal Physiol. 2005;288:F930-8.
- 46. Nedvetsky PI, Tabor V, Tamma G, Beulshausen S, Skroblin P, Kirschner A, et al. Reciprocal regulation of aquaporin-2 abundance and degradation by protein kinase A and p38-MAP kinase. J Am Soc Nephrol. 2010;21:1645-56.
- 47. Moeller HB, Praetorius J, Rutzler MR, Fenton RA. Phosphorylation of aquaporin-2 regulates its endocytosis and protein-protein interactions. Proc Natl Acad Sci U S A;107:424-9.
- 48. Rice WL, Zhang Y, Chen Y, Matsuzaki T, Brown D, Lu HA. Differential, phosphorylation dependent trafficking of AQP2 in LLC-PK1 cells. PLoS One.7:e32843.
- 49. Kato A, Klein JD, Zhang C, Sands JM. Angiotensin II increases vasopressin-stimulated facilitated urea permeability in rat terminal IMCDs. Am J Physiol Renal Physiol. 2000;279:F835-40.
- 50. Klein JD, Frohlich O, Blount MA, Martin CF, Smith TD, Sands JM. Vasopressin increases plasma membrane accumulation of urea transporter UT-A1 in rat inner medullary collecting ducts. J Am Soc Nephrol. 2006;17:2680-6.
- 51. Blount MA, Klein JD, Martin CF, Tchapyjnikov D, Sands JM. Forskolin stimulates phosphorylation and membrane accumulation of UT-A3. Am J Physiol Renal Physiol. 2007;293:F1308-13.
- 52. Blount MA, Mistry AC, Frohlich O, Price SR, Chen G, Sands JM, et al. Phosphorylation of UT-A1 urea transporter at serines 486 and 499 is important for vasopressin-regulated activity and membrane accumulation. Am J Physiol Renal Physiol. 2008;295:F295-9.
- 53. Sands JM, Flores FX, Kato A, Baum MA, Brown EM, Ward DT, et al. Vasopressin-elicited water and urea permeabilities are altered in IMCD in hypercalcemic rats. Am J Physiol. 1998;274:F978-85.
- 54. Zhang C, Sands JM, Klein JD. Vasopressin rapidly increases phosphorylation of UT-A1 urea transporter in rat IMCDs through PKA. Am J Physiol Renal Physiol. 2002;282:F85-90.
- 55. Bansal AD, Hoffert JD, Pisitkun T, Hwang S, Chou CL, Boja ES, et al. Phosphoproteomic profiling reveals vasopressin-regulated phosphorylation sites in collecting duct. J Am Soc Nephrol. 2010;21:303-15.

- 56. Bustamante M, Hasler U, Leroy V, de Seigneux S, Dimitrov M, Mordasini D, et al. Calciumsensing receptor attenuates AVP-induced aquaporin-2 expression via a calmodulin-dependent mechanism. J Am Soc Nephrol. 2008;19:109-16.
- 57. Magno AL, Ward BK, Ratajczak T. The calcium-sensing receptor: a molecular perspective. Endocr Rev. 2011;32:3-30.
- 58. Hippe HJ, Wolf NM, Abu-Taha I, Mehringer R, Just S, Lutz S, et al. The interaction of nucleoside diphosphate kinase B with Gbetagamma dimers controls heterotrimeric G protein function. Proc Natl Acad Sci U S A. 2009;106:16269-74.

Table 1. A list of total proteins decreased in abundance in response to PTH.

All proteins passed two tailed t-test against $log_2(1)$ (P < 0.05) and $log_2(PTH/Control) < -0.58$

RefSeq	Gene	Protein Name	Log ₂ (PTH/	(Control)
	Symbol		Mean	SE
NP_001100650	Ipo9	importin-9	-2.39	0.38
NP_112361	Rpl5	60S ribosomal protein L5	-2.38	0.75
NP_036652	Cat	catalase	-2.24	0.92
NP_001102478	Col6a3	procollagen, type VI, alpha 3 precursor	-2.24	0.42
NP_113986	Slc12a2	solute carrier family 12 member 2	-2.10	0.24
NP_112402	Vim	vimentin	-2.07	0.76
NP_997711	Hspa11	heat shock 70 kDa protein 1-like	-1.80	0.69
NP_037067	Cryab	alpha-crystallin B chain	-1.76	0.45
NP_116002	Lasp1	LIM and SH3 domain protein 1	-1.66	0.56
NP_059024	Pgam2	phosphoglycerate mutase 2	-1.66	0.66
NP_001100678	sept11	septin-11	-1.60	0.28
NP_062230	Ezr	ezrin	-1.49	0.58
XP_213954	Nid1	PREDICTED: nidogen-1	-1.44	0.45
NP_001008525	Ndufs7	NADH dehydrogenase [ubiquinone] iron-sulfur protein 7, mitochondrial	-1.37	0.33
NP_001013951	Atp6v1h	V-type proton ATPase subunit H	-1.33	0.49
NP_001128481	Col4a1	collagen alpha-1(IV) chain precursor	-1.32	0.28
NP_077070	Anxa6	annexin A6	-1.31	0.53
NP_001005889	Rdx	radixin	-1.28	0.42
NP_062249	Ywhag	14-3-3 protein gamma	-1.27	0.53
NP_620203	Podxl	podocalyxin precursor	-1.25	0.42
NP_112274	Anpep	aminopeptidase N precursor	-1.24	0.30
NP_001100389	Arpc2	actin-related protein 2/3 complex subunit 2	-1.20	0.32
NP_001101339	Dysf	dysferlin	-1.19	0.47
NP_036727	Ldhb	L-lactate dehydrogenase B chain	-1.13	0.35
NP_062250	Ywhab	14-3-3 protein beta/alpha	-1.12	0.44
NP_001100089	Usp5	ubiquitin carboxyl-terminal hydrolase 5	-1.11	0.20
NP_786930	Agrn	agrin precursor	-1.09	0.16
NP_001013104	Capg	macrophage-capping protein	-1.08	0.40
NP_058869	Serpinh1	serpin H1 precursor	-1.08	0.41
NP_446423	Rpl6	60S ribosomal protein L6	-1.08	0.33
NP_001098083	Hnrnpa2b1	heterogeneous nuclear ribonucleoproteins A2/B1	-1.06	0.44
NP_001094220	Suclg2	succinyl-CoA ligase [GDP-forming] subunit beta, mitochondrial	-1.05	0.19
NP_062162	Arpc1b	actin-related protein 2/3 complex subunit 1B	-1.05	0.36
XP_001078032	Ahnak	AHNAK nucleoprotein isoform 1	-1.04	0.36
NP_001099367	Cct8	T-complex protein 1 subunit theta	-0.95	0.23
NP_599214	Dexr	L-xylulose reductase	-0.94	0.33
NP_059055	Rab10	ras-related protein Rab-10	-0.93	0.36
NP_058898	Cox4i1	cytochrome c oxidase subunit 4 isoform 1, mitochondrial precursor	-0.90	0.12
NP_062099	Dync1h1	cytoplasmic dynein 1 heavy chain 1	-0.83	0.37
NP_001102874	Rsu1	ras suppressor protein 1	-0.78	0.28
XP_002726232	Slc25a12	calcium-binding mitochondrial carrier protein Aralar1	-0.77	0.22

Table 1.	Continued.
----------	------------

RefSeq Gene		Protein Name	Log ₂ (PTH/Control)	
	Symbol		Mean	SE
XP_002726232	Slc25a12	calcium-binding mitochondrial carrier protein Aralar1	-0.77	0.22
NP_001129231	Col4a3	collagen alpha-3(IV) chain precursor	-0.74	0.15
NP_001004220	Etfb	electron transfer flavoprotein subunit beta	-0.72	0.24
NP_478118	Slc4a7	sodium bicarbonate cotransporter 3	-0.72	0.25
NP_446418	Lamc1	laminin, gamma 1 precursor	-0.70	0.08
NP_001008802	Krt1	keratin, type II cytoskeletal 1	-0.69	0.15
NP_001017461	Ogdh	2-oxoglutarate dehydrogenase, mitochondrial precursor	-0.68	0.21
NP_001013053	Phb2	prohibitin-2	-0.66	0.02
NP_076440	Rab7a	ras-related protein Rab-7a	-0.66	0.25
NP_037106	Lamb2	laminin subunit beta-2 precursor	-0.65	0.15
NP_112644	Vdac2	voltage-dependent anion-selective channel protein 2	-0.63	0.18
NP_001102833	Rab17	ras-related protein Rab-17	-0.62	0.08
NP_446248	F11r	junctional adhesion molecule A precursor	-0.61	0.16
NP_001002016	Lmna	prelamin-A/C isoform C2	-0.60	0.25
NP_001005381	Ddx19a	zinc responsive protein ZD10B	-0.59	0.10
NP_955417	Dld	dihydrolipoyl dehydrogenase, mitochondrial precursor	-0.59	0.22
NP_062090	Map1b	microtubule-associated protein 1B	-0.59	0.11
NP_058718	Itgb1	integrin beta-1 precursor	-0.58	0.20

Table 2. A list of total proteins increased in abundance in response to PTH.

All proteins passed two tailed t-test against $log_2(1)$ (P < 0.05) and $log_2(PTH/Control) < -0.58$

RefSeq	Gene	Protein Name	Log ₂ (PTH	(Control)
	Symbol		Mean	SE
NP_997706	Slc44a4	choline transporter-like protein 4	3.62	1.10
NP_114021	Nme2	nucleoside diphosphate kinase B	2.95	0.41
NP_114184	Psmd1	26S proteasome non-ATPase regulatory subunit 1	2.39	0.89
NP_058973	Ap1b1	AP-1 complex subunit beta-1	1.90	0.51
NP_001102063	Sec23b	protein transport protein Sec23B	1.84	0.49
NP_001124036	Efr3a	protein EFR3 homolog A	1.55	0.21
NP_113806	Nckap1	nck-associated protein 1	1.34	0.16
NP_908939	Ermp1	endoplasmic reticulum metallopeptidase 1	1.24	0.47
NP_085075	Cyb5b	cytochrome b5 type B precursor	1.16	0.48
NP_001026812	Serpinb1a	leukocyte elastase inhibitor A	0.67	0.14
NP_001013241	Pcbp2	poly(rC)-binding protein 2	0.61	0.18

Table 3. A list of phosphoproteins decreased in abundance in response to PTH. All phosphoproteins passed two tailed t-test against $\log_2(1)$ (P < 0.05) and $\log_2(PTH/Control) < -0.58$

Gene	Protein Name	Peptides	Phosphorylation	Log ₂ (PTH/Control)			
symbol			site	Phosphopeptides		Tot prot	
зущоог			Sitt	Mean	SE	Mean	SE
Sec62	translocation protein SEC62	DGEKEDSKKEETPGT*PK	T365	-2.44	0.40	-2.25	1.45
Hnrnpc	heterogeneous nuclear ribonucleoprotein C	NEKS*EEEQSSASVK	S226	-1.71	0.65	1.11	0.77
Lrba	lipopolysaccharide-responsive and beige-like anchor protein	SSVLPSTLTASAPSNAVSVVSSVDSTQVPDAGGESPGS*R	S1715	-1.70	0.65	-0.77	0.47
Cgnl1	cingulin-like protein 1	RQDS*AGPILDGAR	S283	-1.64	0.47	N/A	N/A
Edc4	enhancer of mRNA-decapping protein 4	T*RSPDVISSASTALSQDIPEIASEALSR	T732	-1.64	0.36	N/A	N/A
Cgnl1	cingulin-like protein 1	NCFPKPCGS*QPNS*PTPEDLAK	S198	-1.58	0.49	N/A	N/A
Hdgf	hepatoma-derived growth factor	NSTPS*EPDSGQGPPPEEEEGEEEAAKEEAEAQGVR	S202	-1.58	0.39	N/A	N/A
Prosapip1	proSAP-interacting protein 1	SGHLGSGEGGN#GGLPFAACSPPS*PSALIQELEER	S346	-1.54	0.54	N/A	N/A
Add1	alpha-adducin	EKSPPDQSAVPNT*PPST*PVKLEGGLPQEPTSR	T610	-1.46	0.09	0.47	0.95
Epn3	epsin-3	GS*PSSYTSASSSPR	S175	-1.45	0.24	N/A	N/A
Cgnl1	cingulin-like protein 1	NCFPKPCGS*QPNS*PTPEDLAK	S202	-1.37	0.40	N/A	N/A
Hsp90aa1	heat shock protein HSP 90-alpha	ESDDKPEIEDVGS*DEEEEEKKDGDKK	S263	-1.36	0.24	-0.39	0.38
Dync1li1	cytoplasmic dynein 1 light intermediate chain 1	KPASVSPTTPPS*PTEGEAS	S516	-1.35	0.52	N/A	N/A
Edc4	enhancer of mRNA-decapping protein 4	TRS*PDVISSASTALSQ#DIPEIASEALSR	S734	-1.33	0.12	N/A	N/A
Rbm39	RNA-binding protein 39	DKS*PVREPIDNLTPEER	S136	-1.32	0.37	N/A	N/A
Add1	alpha-adducin	EKSPPDQSAVPNT*PPST*PVKLEGGLPQEPTSR	T614	-1.30	0.05	0.47	0.95
Pxn	paxillin	TGSSS*PPGGLSKPGSQLDSMLGSLQSDLNK	S317	-1.30	0.21	N/A	N/A
Canx	calnexin precursor	QKS*DAEEDGGT*GSQ#DEEDSKPKAEEDEILNR	S553	-1.29	0.56	-0.70	0.56
Mllt4	afadin	SSPNVANQPPS*PGGK	S1189	-1.27	0.39	N/A	N/A
Pxn	paxillin	T*GSSSPPGGLSKPGSQLDSMLGSLQSDLNK	T313	-1.17	0.25	N/A	N/A
Myh9	myosin-9	GTGDCS*DEEVDGKADGADAK	S1944	-1.13	0.44	-0.23	0.28
Gtpbp1	GTP-binding protein 1	SRS*PVDSPVPASMFAPEPS*SPGAAR	S8	-1.09	0.07	N/A	N/A
Prkar2a	cAMP-dependent protein kinase type II-alpha regulatory subunit	RVS*VCAETFNPDEEEDNDPR	S97	-1.07	0.34	N/A	N/A
Pqcp	interferon regulatory factor 2-binding protein-like	KAS*PEPPDSAESALK	S534	-1.07	0.36	N/A	N/A
Arfgef2	brefeldin A-inhibited guanine nucleotide-exchange protein 2	ELEKPIQSKPQSPVIQATAGS*PK	S227	-1.05	0.23	N/A	N/A
Trim28	transcription intermediary factor 1-beta	SRS*GEGEVSGLM@R	S474	-1.05	0.26	N/A	N/A
Zbtb20	zinc finger and BTB domain-containing protein 20	EGQVEAAQPEQAAEAPAESSAQPNQLETGASS*PER	S359	-1.04	0.42	N/A	N/A
Usp8	ubiquitin carboxyl-terminal hydrolase 8	SYS*SPDITQALQEEEKR	S681	-1.03	0.38	N/A	N/A
Lmo7	LIM domain only protein 7	S*KSLSDVSAEDVQSLR	S650	-1.03	0.39	N/A	N/A
Slc9a1	sodium/hydrogen exchanger 1	SKEPSSPGTDDVFTPGPSDS*PGSQR	S790	-1.03	0.33	N/A	N/A
Ppp1r11	protein phosphatase 1 regulatory subunit 11	AFGESSTES*DEDEEEGCGHTHCVR	S78	-1.02	0.18	N/A	N/A
Arfgef2	brefeldin A-inhibited guanine nucleotide-exchange protein 2	ELEKPIQSKPQS*PVIQAT*AGSPK	S218	-1.00	0.32	N/A	N/A
Arrb1	beta-arrestin-1	GM@KDDKDEEDDGTGS*PHLNNR	S412	-0.99	0.36	N/A	N/A
Hsp90ab1	heat shock protein HSP 90-beta	IEDVGS*DEEDDSGKDK	S255	-0.98	0.31	-0.26	0.26
Plec	plectin isoform 1a	RTSS*EDNLYLAVLR	S21	-0.95	0.06	N/A	N/A
Pak2	serine/threonine-protein kinase PAK 2	YLS*FTPPEKDGFPSGTPALNTK	S141	-0.89	0.14	N/A	N/A
Matr3	matrin-3	SYS*PDGKES*PSDKK	S598	-0.88	0.23	-0.19	0.57
Epn3	epsin-3	GKSPS*PVELDPFGDSSPSCK	S419	-0.84	0.23	N/A	N/A

Table 3. continued

Gene	Protein Name	Protein Name Peptides		Log ₂ (PTH/Control)			
symbol			site			Tota prote	
				Mean	SE	Mean	SE
Sfrs2	serine/arginine-rich splicing factor 2	VDNLTYRT*SPDTLR	T25	-0.84	0.28	N/A	N/A
Lmo7	LIM domain only protein 7	S*TTELNDPLIEK	S1476	-0.82	0.24	N/A	N/A
Matr3	matrin-3	SYS*PDGKES*PSDKK	S604	-0.82	0.24	-0.19	0.57
Ebag9	receptor-binding cancer antigen expressed on SiSo cells precursor	KLS*GDQITLPTTVDYSSVPK	S36	-0.82	0.28	N/A	N/A
Gstm2	glutathione S-transferase Mu 2	LQLAMVCYS*PDFER	S117	-0.80	0.13	-0.33	0.14
Fam83h	protein FAM83H	GS*PTPAYPER	S860	-0.74	0.29	N/A	N/A
Fam83h	protein FAM83H	KGS*PTPAYPER	S882	-0.74	0.29	N/A	N/A
Map4	microtubule-associated protein 4	VTEFNNVTPLSEEEVASIKDVS*PSPETETAK	S520	-0.74	0.04	-0.59	0.60
Lrrfip2	leucine-rich repeat flightless-interacting protein 2	RGS*GDTSSLIDPDTSLSELR	S133	-0.72	0.07	N/A	N/A
Canx	calnexin precursor	SDAEEDGGT*GSQDEEDSKPKAEEDEILNR	T561	-0.71	0.10	-0.70	0.56
Aqp2	aquaporin-2	RQ#S*VELHSPQSLPR	S256	-0.68	0.12	-1.07	0.57

Supplement table 1. A list of phophopeptides newly identified.

RefSeq	Gene	Protein Name	Peptides	Phosphorylation
	symbol			site
NP_001004447	Spata21	spermatogenesis-associated protein 21	PPVLPT*VPR	T223
NP_001007000	Xrcc4	DNA repair protein XRCC4	YMDELRRALVPES*GAAGAY*K	S78, Y84
NP_001007236	Itpr1	inositol 1,4,5-trisphosphate receptor type 1 isoform 1	VT*LDEAGNEGSWFYIQPFYK	T150
NP_001007697	mrpl9	39S ribosomal protein L9, mitochondrial	VPMSVVLFRKPKTKRY*K	Y245
NP_001007702	Tram1	translocating chain-associated membrane protein 1	KGTENGVNGT*VTSNGADSPR	T357
NP_001008330	RGD1311745	uncharacterized protein KIAA1143 homolog	IQPQLPDEDGNES*DKEDEQPQVVVLK	S50
NP_001008345	Etf1	eukaryotic peptide chain release factor subunit 1	LVDISYGGENGFNQAIELST*EVLS*NVK	T272, S276
NP_001010962	Rps6kb2	ribosomal protein S6 kinase beta-2	AVDWWSLGALMYDMLT*GS*PPFTAENR	T264, S266
NP_001011894	Psme3	proteasome activator complex subunit 3	T*VT*EIDEKEYISLR	T205, T207
NP_001012191	Dtnb	dystrobrevin beta	AQATGS*PHTS*PTHGGGR	T527, S528
NP_001013884	Ccdc45	centrosomal protein of 95 kDa	SAS*EQFCR	S125
NP_001014098	Nol10	nucleolar protein 10	RRIELIQDFEMPT*	T53
NP_001014221	Atp6v1c2	V-type proton ATPase subunit C 2	S*T*KLIAEDNEGGLFTVT*LFRK	S211, T212, T227
NP_001017462	LOC361346	lung adenoma susceptibility protein 2 homolog precursor	DLVDDTSGRQS*PK	S362
NP_001020142	Haus8	HAUS augmin-like complex subunit 8	VVESRY*LQY*DKKTKK	Y38, Y41
NP_001020143	Arglu1	arginine and glutamate-rich protein 1	AS*SPPDRIDIFGR	S74
NP_001020199	Fam35a	uncharacterized protein LOC364514	MTVSQETAS*LMST*ANTWEK	S28, T32
NP_001020222	Fam110c	protein FAM110C	KPLRPDSLVIY*RQKCEFVRGSDADSSRVGLMK	Y103
NP_001020796	Stub1	STIP1 homology and U-Box containing protein 1	LGT*GGGSPDKSPSAQELK	T15
NP_001020858	Dclre1b	5' exonuclease Apollo	HSS*Y*SELR	S278
NP_001025072	Csflr	macrophage colony-stimulating factor 1 receptor precursor	IY*SIMQSCWDLEPT*K	Y928, T940
NP_001029253	Paqr7	progestin and adipoQ receptor family member VII	LDIS*PVVHR	S218
NP_001030094	Atad3a	ATPase family AAA domain-containing protein 3	SLYRNVLMYGPPGT*GK	T355
NP_001032170	Akap9	A-kinase anchor protein 9	NS*S*PDEVLVSNMDTSR	S1500, S1501
NP_001032882	Dock8	dedicator of cytokinesis 8	VMS*S*SNPDLAGTHCAADEEVKNIMSSK	S902, S903
NP_001034112	Net1	neuroepithelial cell-transforming gene 1 protein	VRFQDPS*PGQSHTLQANDVFHK	S420
NP_001037747	Mat2b	methionine adenosyltransferase 2 subunit beta	YEMACAIADAFNLPSSHLRPITDS*PVIGAQRPK	S282
NP_001041365	Naa25	N-alpha-acetyltransferase 25, NatB auxiliary subunit	IRS*LTLR	S691
NP_001092980	Vom2r51	vomeronasal 2 receptor 51 precursor	FILT*RVIVAFGDT*YSLLR	T271, T280
NP_001093988	Hs2st1	heparan sulfate 2-O-sulfotransferase 1	LEES*RAKLERAIARHEVR	S37
NP_001094040	Myst3	histone acetyltransferase KAT6A	QKQRPS*EER	S28
NP_001094110	Lamc2	laminin, gamma 2 precursor	LSLAESEASLQNTNIHS*S*EHYVGPNGFK	S746, S747
NP_001094189	Ap3d1	AP-3 complex subunit delta-1	VDIITEEMPENALPSDEDDKDPNDPY*R	Y795
NP_001094198	Ccdc43	coiled-coil domain-containing protein 43	KAALLAQYADVT*DEEDEADEKADPGASTANIGSDK	T137
NP_001094258	LOC498222	specifically androgen-regulated gene protein	SS*FHS*HPQNWLSNHTEATDSGPVSSLQEQR	S317, S320
NP_001094316	Mtmr10	myotubularin related protein 10	RNS*LILK	S603
NP_001094479	Tlr8	toll-like receptor 8 precursor	VIY*LSGNRIASVIDGTDHS*SWR	Y416, S432
NP_001099214	Eif2ak4	eukaryotic translation initiation factor 2-alpha kinase 4	HERPAVPGT*PPPDYIPQAQNSSATGGK	T667
NP_001099225	Pkn2	serine/threonine-protein kinase N2	AS*SLGEIDDSSELR	S581
NP_001099458	Plxna2	plexin-A2	VSDRS*VVALVPK	S1593
NP_001099467	Mrpl1	39S ribosomal protein L1, mitochondrial	ESEPEDDVY*LKR	Y89
NP_001099470	Cox18	mitochondrial inner membrane protein COX18	FQMY*VTNFVR	Y252
NP_001099577	Snrnp48	U11/U12 small nuclear ribonucleoprotein 48 kDa protein	RRLQEELSEFVES*CCRT*L	S24, T28
NP_001099624	Tmco6	transmembrane and coiled-coil domain-containing protein 6	TLVGLLT*S*NR	T118, S119
NP_001099893	Mecom	MDS1 and EVI1 complex locus protein EVI1	NFIGNSNHGSQS*PR	S727
NP_001100124	Sec61b	protein transport protein Sec61 subunit beta	PGPTPSAT*NVGS*SGRSPSK	T9, S13
NP_001100546	Rab40b	ras-related protein Rab-40B	TIRPPQS*PPR	S266
NP_001100939	Zc3h12d	probable ribonuclease ZC3H12D	VVCY*DDRYIVK	Y181
NP_001101709	Gtf3c3	general transcription factor 3C polypeptide 3	GKSS*PKENPGDAEVPSSSGIDSAK	S43
NP_001101927	Ppil4	peptidyl-prolyl cis-trans isomerase-like 4	INHTVILDDPFDDPPDLLIPDRS*PEPT*KEQLDSGR	S178, T182
NP_001102048	Aif11	allograft inflammatory factor 1-like	ANESS*PKPAGPPPER	S134
NP_001102128	Topors	E3 ubiquitin-protein ligase Topors	DSSWSRRSQTLS*LSSGSTSRSRS*R	S662, S673
NP_001102186	Dcaf4	DDB1- and CUL4-associated factor 4	VEIQSSDPS*ALAS*DR	S167, S171
NP_001102270	Klf7	Krueppel-like factor 7	TRTHT*LSHT*DPHTY	T45, T49
NP_001102754	LOC500797	uncharacterized protein LOC500797	AESPET*PKETPIER	T258
NP_001102734 NP_001102808	Slc35f1	solute carrier family 35 member F1	Y*MILGFIDLEANY*LVVK	Y132, Y144
NP_001103355	Fam129b	niban-like protein 1	DSVVLHNS*DPNLH	S574
NP_001103355	Fam129b	niban-like protein 1	TVLEAS*PPASPLR	S693
NP_001103333	Tmprss13	transmembrane protease serine 13	VY*LVRAIPVGTVIRASPAR	Y93
-11_001121000	p		Briam (Grinabirin	1/3

Supplement table 1 (continue)

RefSeq	Gene	Protein Name	Peptides	Phosphorylation
	symbol			site
NP_001121010	Spire2	protein spire homolog 2	ELS*PQLER	S126
NP_001121020	Traf7	E3 ubiquitin-protein ligase TRAF7	VWDT*CT*TYKCQK	T424, T426
NP_001121023	Lrch4	leucine-rich repeat and calponin homology domain-containing protein 4	PLGSIQRPNS*FLFR	S509
NP_001121109	Snx9	sorting nexin 9	SSS*PYFKDSEPAEAGGIQR	S175
NP_001124008	Fzd6	frizzled-6 precursor	SSVSEGAPSEGRVS*PK	S659
NP_001128117	Cntrob	centrobin	LEHGGT*DGQGELVPRRNTDSRLGEIT*RK	T835, T855
NP_001158128	Fcgbpl1	Fc fragment of IgG binding protein-like precursor	HRSSNKVS*Y*VR	S110, Y111
NP_001171290	LOC100362110	uncharacterized protein LOC100362110	QHQDHHST*R	T518
NP_001182488	Camta1	calmodulin binding transcription activator 1 isoform 1	TRPQNGS*MILYNRKK	S106
NP_001182528	RGD1559980	uncharacterized protein LOC499158	INY*MQNLKKEKRK	Y38
NP_001258265	RGD1565800	V-set and immunoglobulin domain-containing protein 10 precursor	GQDMGDVMVLVDS*EEEEEEEENKGALAEVVGQETR	S486
NP_036899	Gnrh1	progonadoliberin-1 precursor	RNT*EHLVDS*FQEMGK	T38, S44
NP_064477	Sfrs12	splicing regulatory glutamine/lysine-rich protein 1	SRSRQKDRARS*K	S238
NP_071783	Fxyd4	FXYD domain-containing ion transport regulator 4 precursor	NHTPSSLPEKVT*PLITPGSAST*	T77, T87
NP_113905	Amotl2	angiomotin-like protein 2	GGAGAGGTGS*PQASLEIGAPEDS*QVLQQATR	S50, S63
NP_113940	Bcam	basal cell adhesion molecule precursor	GAPPAREPELSHSGS*ERPEHTGLLMGGPSGGGR	S596
NP_114013	Fbn1	fibrillin-1 precursor	GGPEPPAS*GEMDDNSLSPEACYECK	S2703
NP_445873	Arid4b	AT-rich interactive domain-containing protein 4B	GKGTNSSDSEDLS*AGES*VTK	S1075, S1079
NP_445899	Hdac2	histone deacetylase 2	MLPHAPGVQMQAIPEDAIPEES*GDEDEEDPDKR	S394
NP_446307	Akap8	A-kinase anchor protein 8	NEAAVPAAAAGS*PVPVIAIPGILEDELEQTDAEAKDTPTE	S659
NP_446418	Lamc1	laminin, gamma 1 precursor	S*QECYFDPELYR	S346
NP_598198	Mmp10	stromelysin-2 precursor	FDET*RQLMDKGFPR	T413
NP_599205	Sulf1	extracellular sulfatase Sulf-1 precursor	FRT*NKKAKIWRDTFLVER	T400
NP_620194	Tmem49	vacuole membrane protein 1	EQHNGS*FTDPSSVNEK	S23
NP_620793	Phrf1	PHD and RING finger domain-containing protein 1	AQRPS*PPDPWDDEDGVSCTPFFGSEER	S736
NP_783187	Ssx2ip	afadin- and alpha-actinin-binding protein	SKEAKRELS*IVALLNCMNELLVLQR	S95
NP_853669	Tbx3	T-box transcription factor TBX3	RMYIHPDSPATGEQWMS*K	S199
XP_001054169	LOC679718	PREDICTED: rCG41835-like	QHFWGMWNAGRET*S*TPGTELSENQAKK	T77, S78
XP_001054445	LOC679782	PREDICTED: histocompatibility 60a	AQQLQHNCSLS*T*GPK	S301, T302
XP_001056343	Srrm2	PREDICTED: serine/arginine repetitive matrix protein 2	DKFS*PTQDRPESSTVLKDTPR	S1153
XP_001056343	Srrm2	PREDICTED: serine/arginine repetitive matrix protein 2	AAEIPAVASCWVGPQVS*PEHK	S1271
XP_001056343	Srrm2	PREDICTED: serine/arginine repetitive matrix protein 2	ELS*HS*PPRDNSFESLEFR	S1278, S1280
XP_001056343	Srrm2	PREDICTED: serine/arginine repetitive matrix protein 2	NSGPVLEVNTDFS*PEVKEELNGPFLNQTETDPSLDMK	S1306
XP_001056343	Srrm2	PREDICTED: serine/arginine repetitive matrix protein 2	IHTTSLTGQS*PPLASGHQGEVDAPSEPGATNIQQPS*SPDPSTK	S295, S321
XP_001056343	Srrm2	PREDICTED: serine/arginine repetitive matrix protein 2	IHTTSLTGQS*PPLASGHQGEVDAPSEPGATNIQQPSS*PDPSTK	S295, S322
XP_001056343	Srrm2	PREDICTED: serine/arginine repetitive matrix protein 2	SSTGPELPAPT*PLLVEQHGDSPRPLAAIPSSQEPVNPSS*EASPTR	S392
XP_001056343	Srrm2	PREDICTED: serine/arginine repetitive matrix protein 2	SSTGPELPAPTPLLVEQHGDSPRPLAAIPSSQEPVNPSSEAS*PTR	S395
XP_001056343	Srrm2	PREDICTED: serine/arginine repetitive matrix protein 2	DKFSPT*QDRPESSTVLKDTPR	T1155
XP_001056343	Srrm2	PREDICTED: serine/arginine repetitive matrix protein 2	IHT*TSLTGQSPPLASGHQGEVDAPSEPGATNIQQPSS*PDPSTK	T288
XP_001056343	Srrm2	PREDICTED: serine/arginine repetitive matrix protein 2	IHTTSLT*GQSPPLASGHQGEVDAPSEPGATNIQQPSS*PDPSTK	T292
XP_001056343	Srrm2	PREDICTED: serine/arginine repetitive matrix protein 2	SSTGPELPAPT*PLLVEQHGDSPRPLAAIPSSQEPVNPSS*EASPTR	T364
XP_001056911	LOC681458	PREDICTED: acyl-CoA desaturase 1-like	ITEPPS*GVMQK	S16
XP_001058594	LOC681825	PREDICTED: prefoldin subunit 3-like	NLEALEDDLDFLRDQFTTT*EVS*IL	T169, S172
XP_001061636	LOC682469	PREDICTED: lysine-specific demethylase 3B-like	S*SSPTSSLTQPIEMPTLSSS*PTEERPTVGPGQQDNPLLK	S726
XP_001061900	Hist1h4m	PREDICTED: histone cluster 1, H4m	MEY*LTAEILELAGNAAR	Y58
XP_001066275	LOC360713	PREDICTED: pleckstrin homology-like domain, family B, member 2-like	KGS*LQDVDIAGFGSLGHSASFLAPR	S555
XP_001066711	LOC683603	PREDICTED: zinc finger and SCAN domain-containing protein 2-like	WLRPEVHT*KEQMLTVLPR	T93
XP_001068576	LOC684024	PREDICTED: dual specificity phosphatase 28-like	TAY*LMRHR	Y109
XP_001078719	LOC687472	PREDICTED: WD repeat-containing protein 87-like	EAT*EVKETLIDKWTLGVK	T1198
XP_002725915	LOC100364027	PREDICTED: putative hexokinase HKDC1-like	ILIDLTRQGLLFRGQIS*ERLRTR	S711
XP_002726316	RGD1561878	PREDICTED: putative Polycomb group protein ASXL1-like	WYLVTVNIS*NR	S23
XP_002729192	LOC100360302	PREDICTED: protein transport protein Sec16A-like	DNYAY*S*DRPEK	Y1294, S1295
XP_578715	LOC503192	PREDICTED: zinc finger protein ZFP	MAAGSPKS*RLR	S8

Figure legends

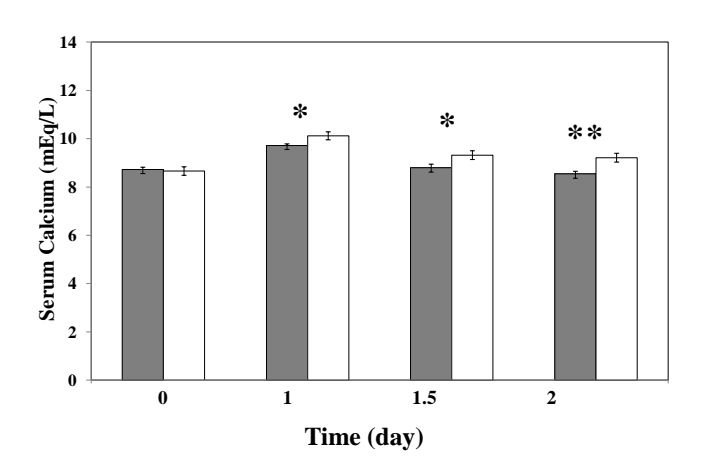


Figure 1. Effect of PTH on serum Ca. Serum Ca of rats treated with 15ug/kg/day of PTH (PTH, \Box , n=7) and control rats (C, \blacksquare , n=7) was significantly higher in PTH than in controls at day 1, 1.5 and 2 (*, P \leq 0.05).

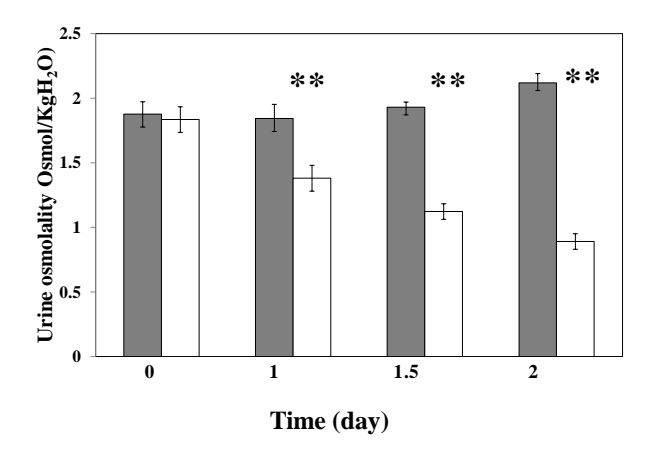


Figure 2. Effect of PTH on urine osmolality. Urine osmolality of rats treated with 15 ug/kg/day of PTH (PTH, \square , n=7) was significantly lower than those of control rats (C, \blacksquare , n=7) at 1 day (**, P<0.01). Urine osmolality of P remained decreased until 2 days of experiment.

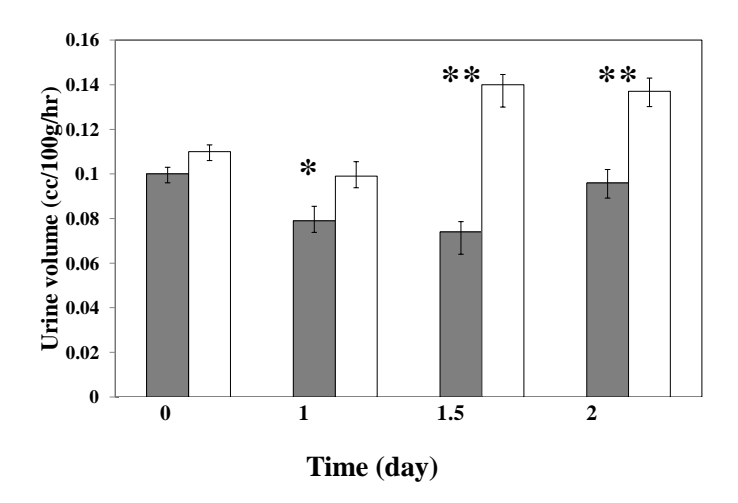


Figure 3. Effect of PTH on urine volume. Urine volume of rats treated with 15ug/kg/day of PTH (PTH, \Box , n=7) was significantly higher than those of control rats (C, \blacksquare , n=7) at 1 days (*, P<0.05).

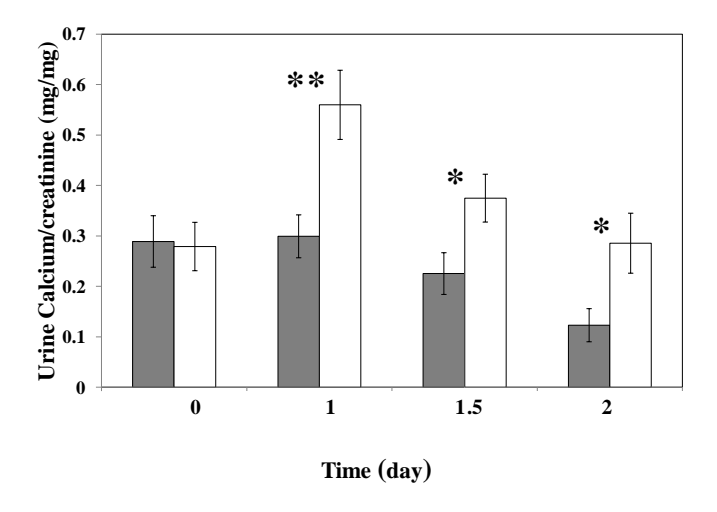


Figure 4. Effect of PTH on urine calcium excretion. Urine calcium/creatinine of rats treated with 15ug/kg/day of PTH (PTH, \Box , n=7) was significantly higher than those of control rats (C, \blacksquare , n=7) at 1 days (**, P<0.01).

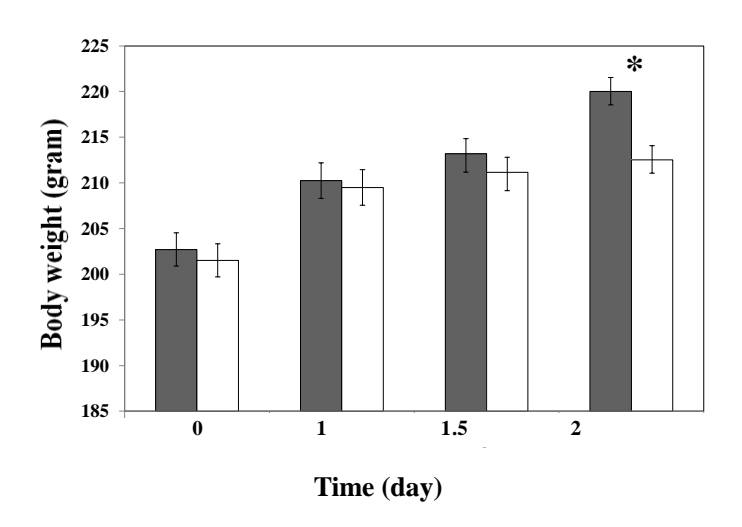


Figure 5. Effect of PTH on body weight. Body weight of rats treated with 15ug/kg/day of PTH (PTH, \Box , n=7) was significantly lower than those of control rats (C, \blacksquare , n=7) at 2 days

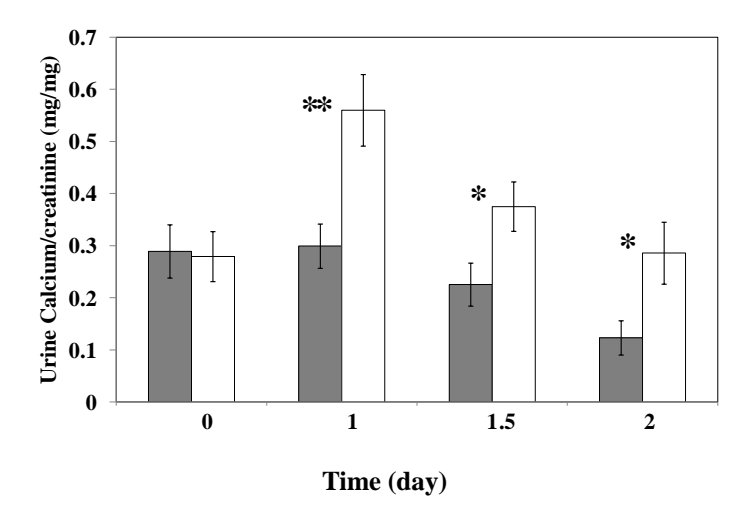


Figure 6. Effect of PTH on urine calcium to creatinine ratio. Rats treated with 15ug/kg/day of PTH (+, PTH, n=7) significantly excreted more calcium in urine than controls (C, \square , n=7) as demonstrated by U calcium to creatinine ratio since 1 day through 2 days of experiment (*, P<0.05; **, P<0.005).

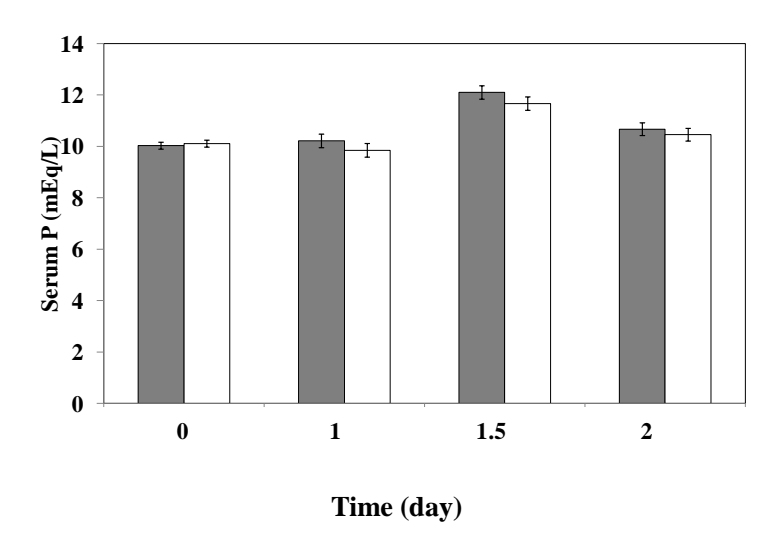


Figure 7. Effect of PTH on serum P. Serum P of rats treated with 15ug/kg/day of PTH (+, PTH, n=7) did not significantly differ from those of controls (C, □, n=7) during 2 days of experiment.

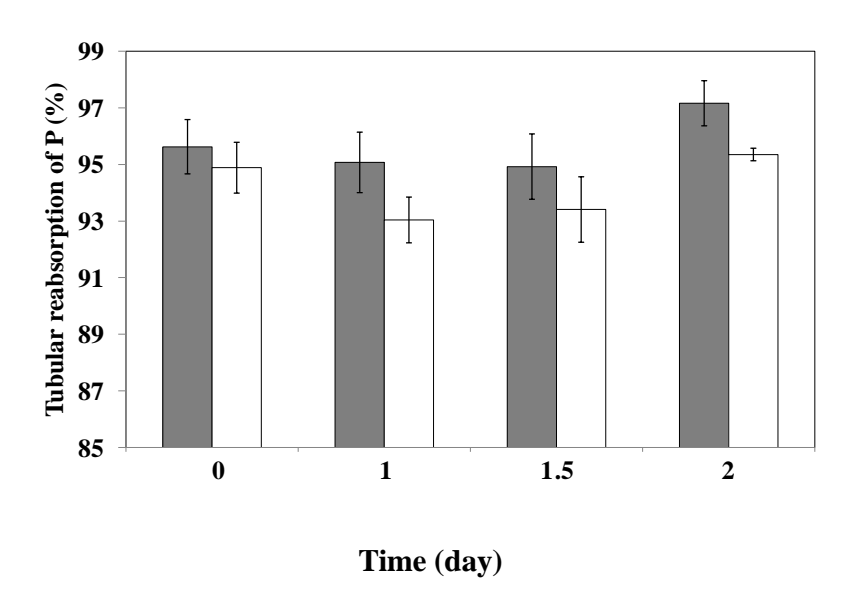


Figure 8. Effect of PTH on tubular reabsorption of P. Serum P of rats treated with 15 ug/kg/day of PTH (+, PTH, n=7) did not significantly differ from those of controls (C, \square , n=7) during 2 days of experiment.

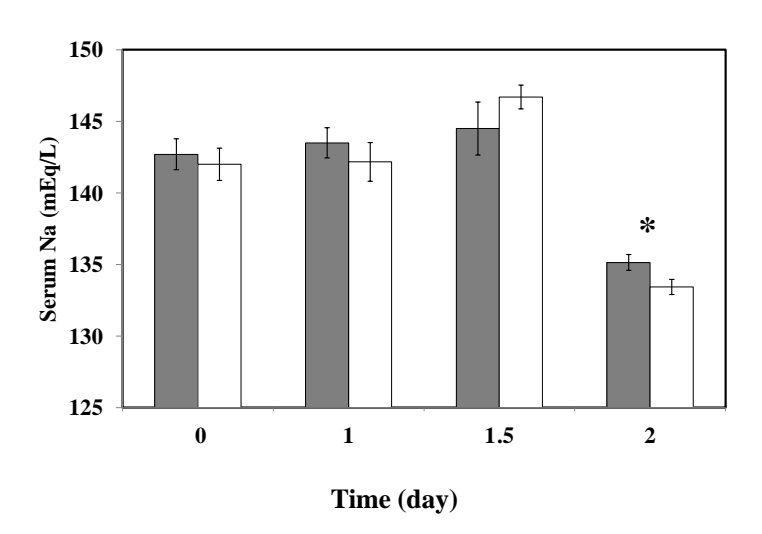


Figure 9. Effect of PTH on serum Na. Serum Na of rats treated with 15ug/kg/day of PTH (+, PTH, n=7) significantly lower than those of controls (C, \square , n=7) on day 2 of experiment (*, P<0.05.

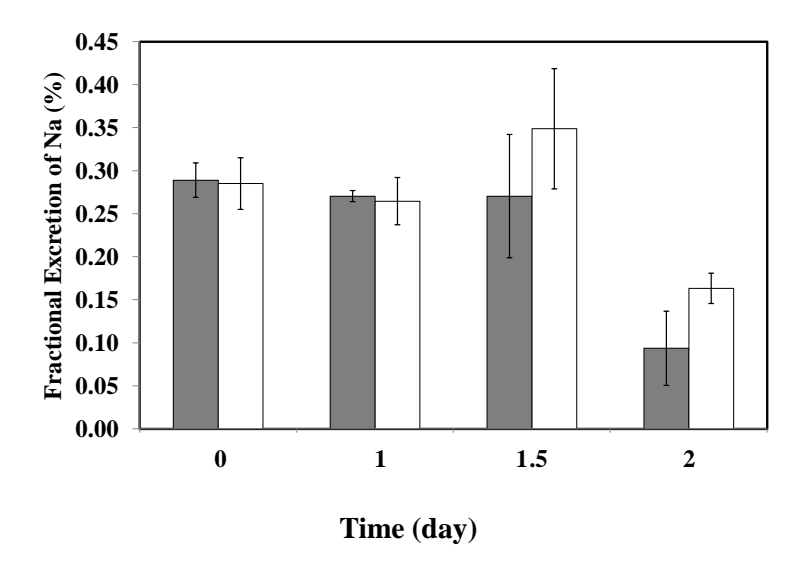


Figure 10. Effect of PTH on fractional excretion of Na. Rats treated with 15ug/kg/day of PTH (+, PTH, n=7) excreted more Na in urine than controls (C, \Box , n=7) on 1.5-2 days of experiment, but these did not reach statistically significant difference.

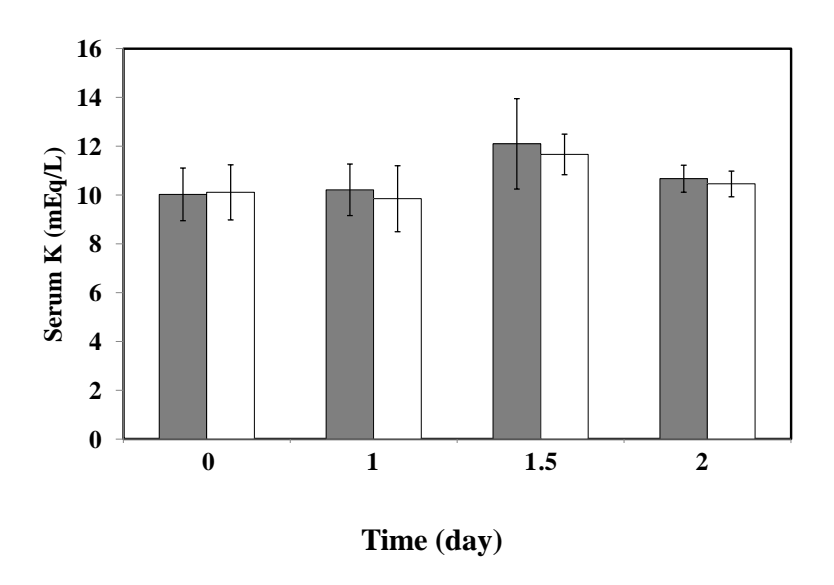


Figure 11. Effect of PTH on serum K. Serum K of rats treated with 15ug/kg/day of PTH (+, PTH, n=7) was not different from those of controls (C, \square , n=7).

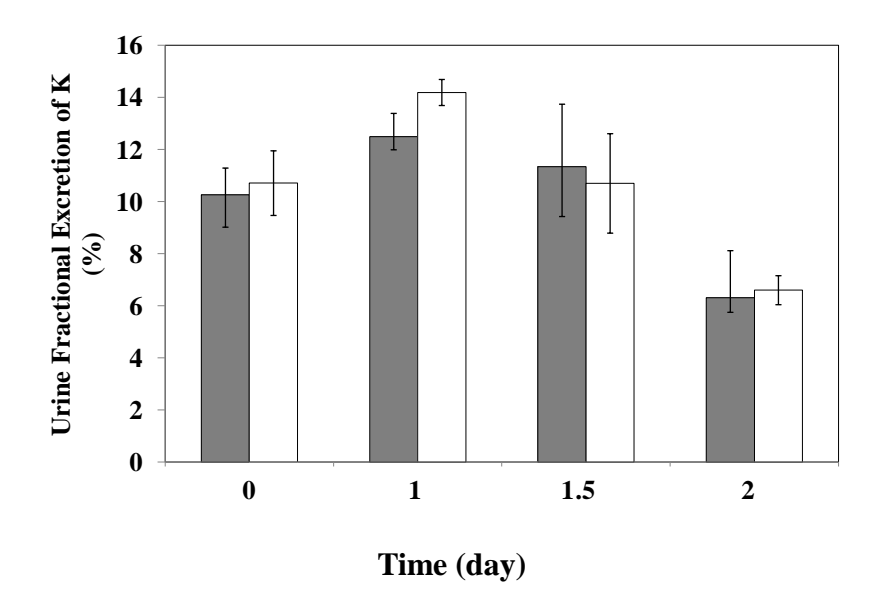


Figure 12. Effect of PTH on urine fractional excretion of K. Rats treated with 15ug/kg/day of PTH (+, PTH, n=7) did not had urine excretion of K differ from controls (C, \Box , n=7).

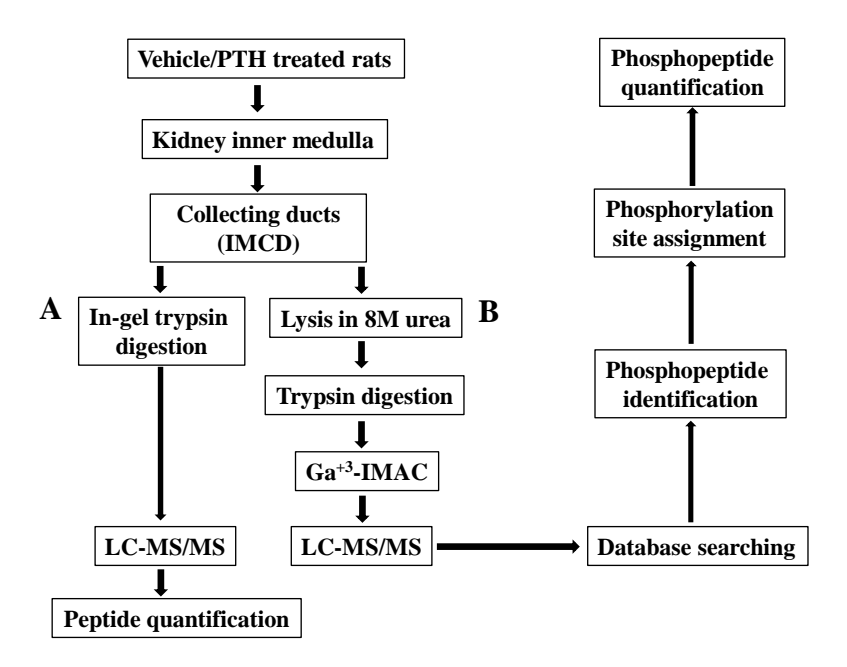


Figure 13. Overview of proteomics and phosphoproteomics profiling of native rat inner medullary collecting duct (IMCD). (A) Experiment workflow for quantitative proteomic analysis with in-gel trypsin digestion. (B) Experiment workflow for quantitative phosphoproteomic analysis with in-solution trypsin digestion and phosphopeptide enrichment with immobilized metal affinity chromatography (IMAC). Four datasets were analysed by InsPecT and SEQUEST search engines followed by assignment of phosphorylation sites using PhosSa program.

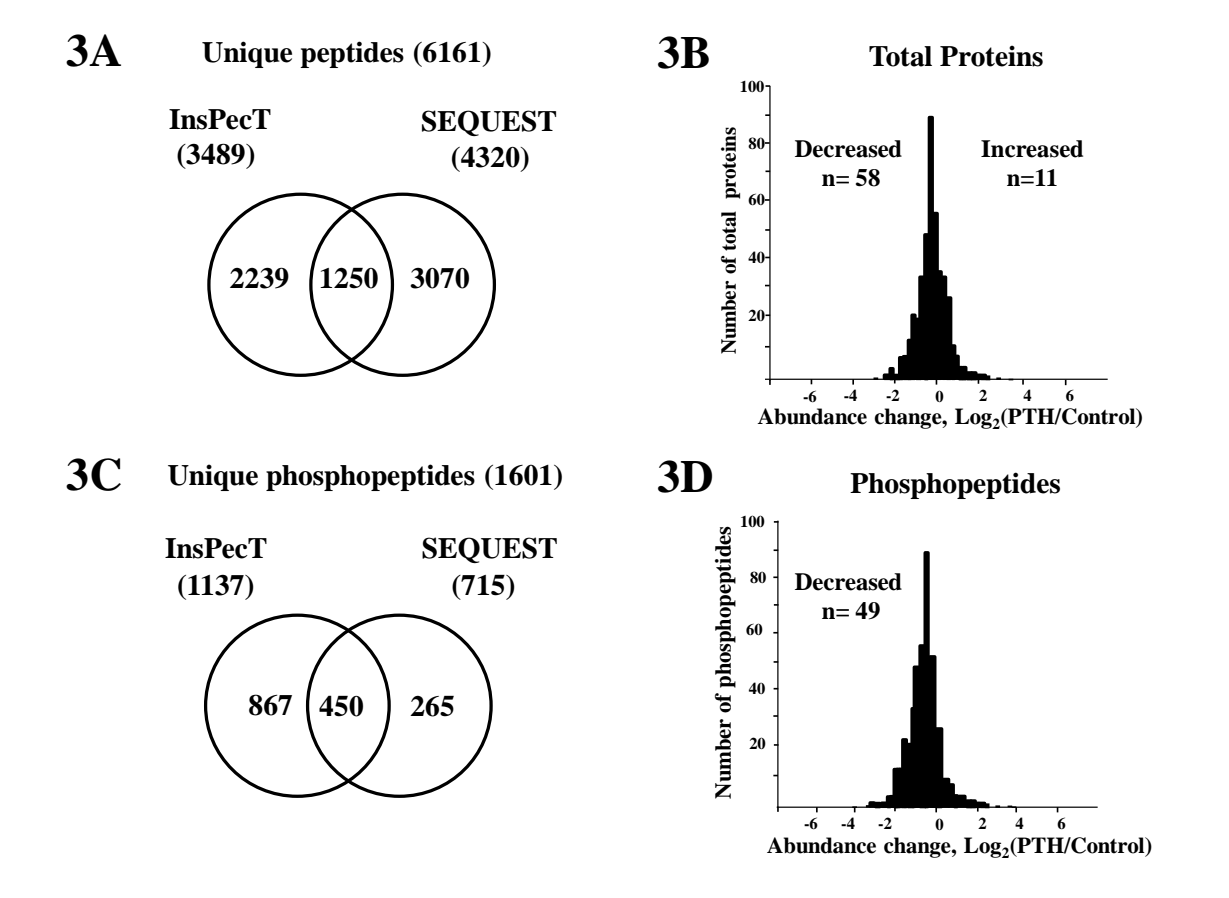


Figure 14. Peptides and Phosphopeptides identified in IMCD cells. (A) Venn diagram of peptides identified by two search alogrithms (SQUEST, and InsPecT). Numbers are unique peptides identified. (B) Distribution of changes for all quantified proteins identified at least 3 experiments. Numbers are changed peptides meeting dual criteria (|log2[PTH/control]| less than 0.58 and passed two tailed t-test against log₂(1) with P<0.05) (C) Venn diagram of phosphopeptides identified by two search alogrithms. Numbers are unique phosphopeptides identified. (D) Distribution of changes for all quantified proteins identified at least 3 experiments. Number is decreased phosphopeptides which meeting 2 criteria as above.

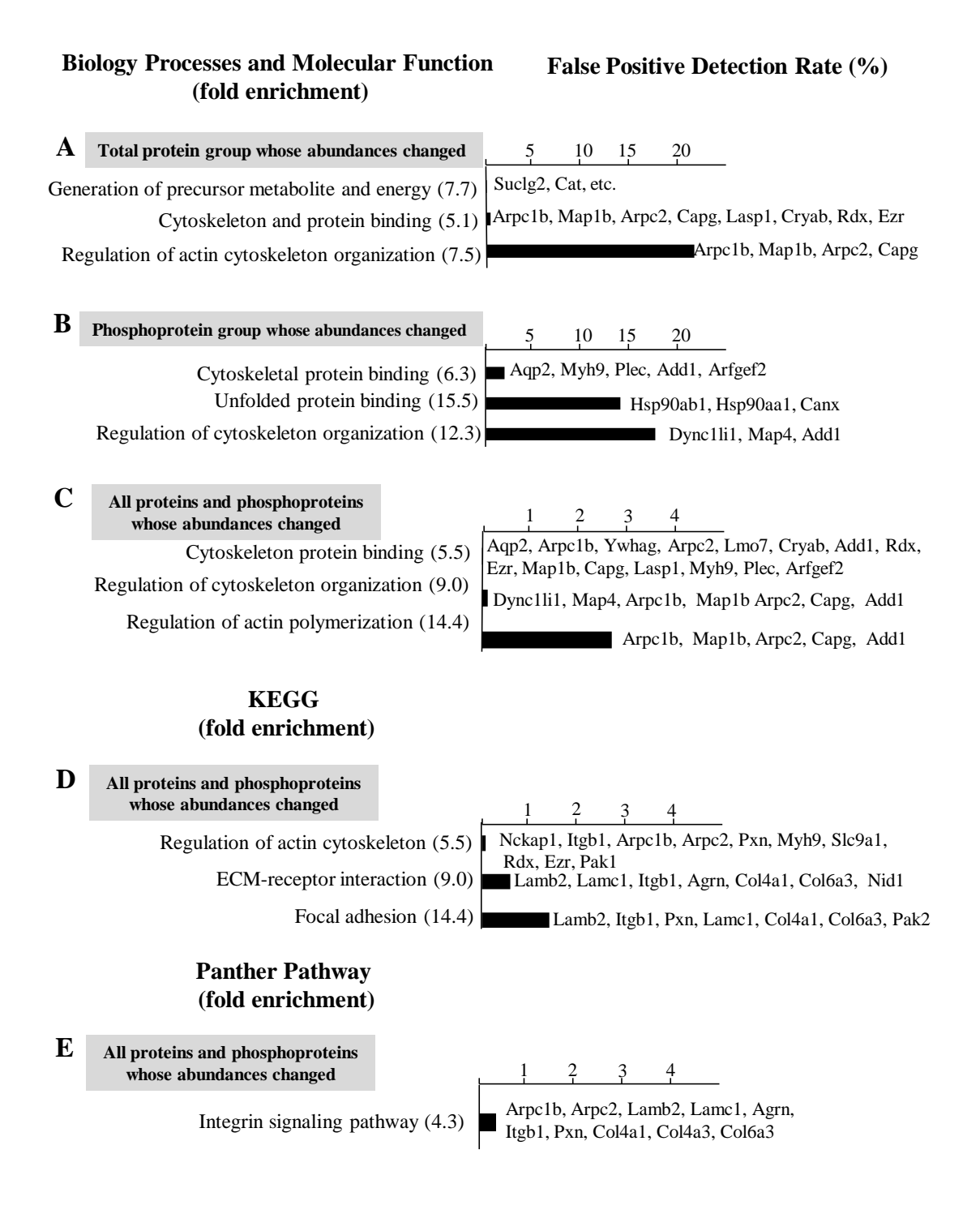


Figure 15. Gene Ontology biological process and molecular function analysis and database search genomes (KEGG). David bioinformatic suite was employed to identified proteins and phosphoproteins that changing in abundances in response to hypercalcemia and meeting 2 criteria as above. GO terms and KEGG listed were significant enriched (P<0.05, Fisher exact

test). (A) GO terms enriched among 69 proteins that changing in abundances. (B) GO terms enriched among 49 phosphopeptides that changing in abundances. (C) GO terms enriched among 118 proteins and phosphoproteins that changing in abundances. (D) KEGG enriched among 118 proteins and phosphoproteins that changing in abundances. (E) Panther pathway enriched among 118 proteins and phosphoproteins that changing in abundances.

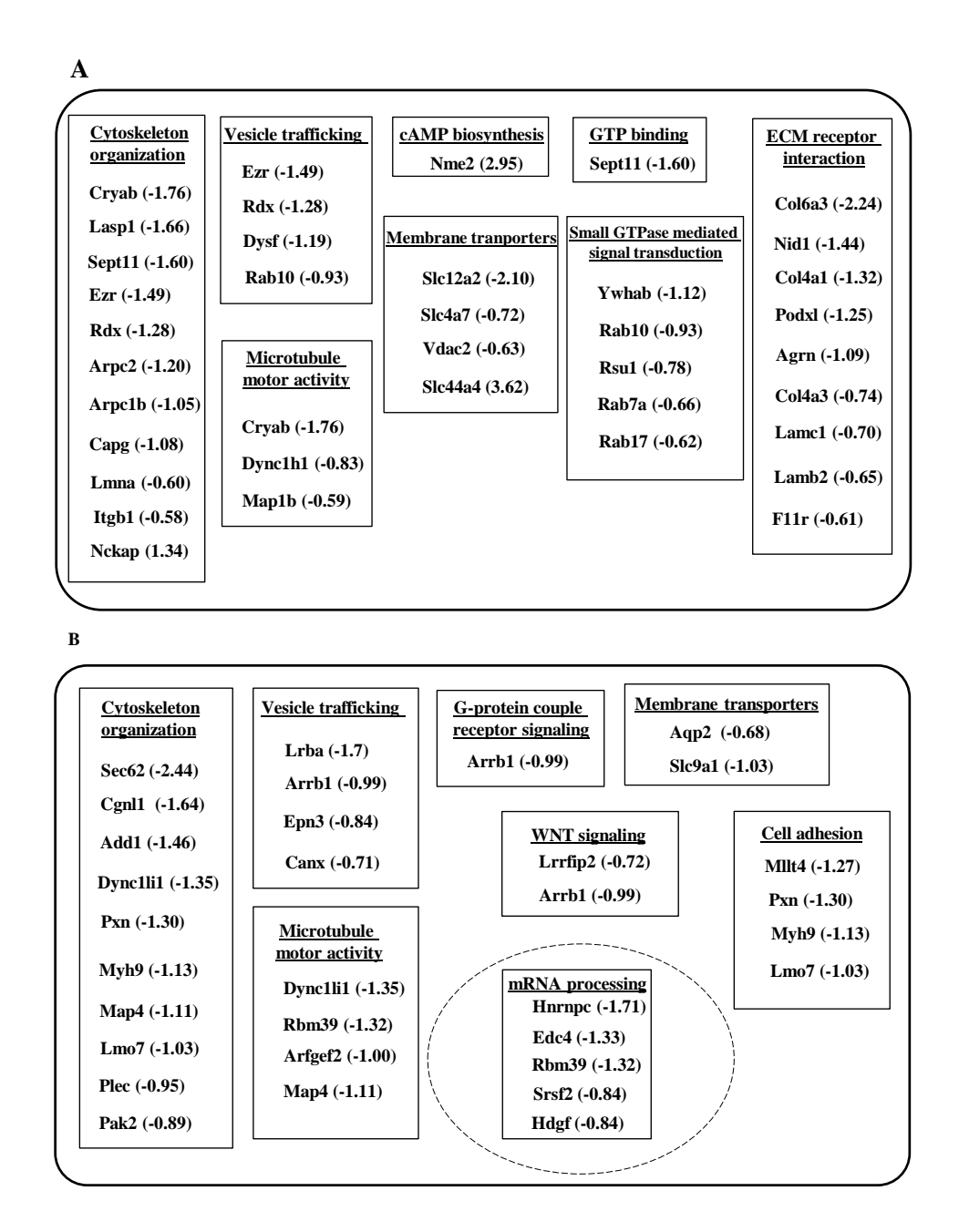


Figure 16. Proteins and phosphoproteins changing in IMCD in response to hypercalcemia. Protein (A) and phosphoproteins (B) groupings were hand curated based on Gene Ontology biological and functional process. Quantification results are given in parentheses as average log₂(PTH/Vehicle) for proteins and phosphoproteins meeting dual criteria (|log2[PTH/control]| less than 0.58 and passed two tailed t-test against log₂(1) with P<0.05).

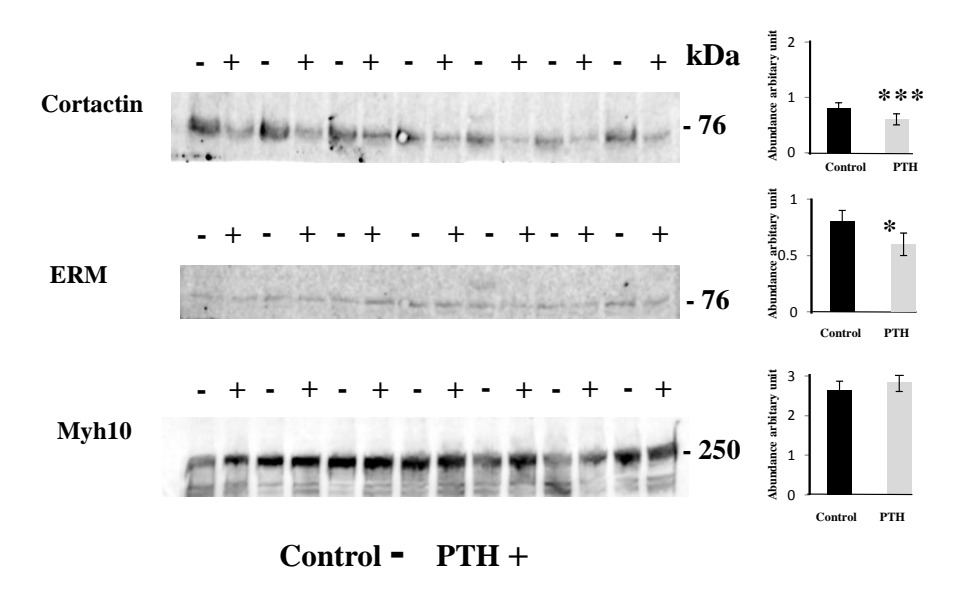


Figure 17. Confirmation of hypercalcemia regulated actin cytoskeletal organization and integrin signaling pathway by immunoblotting. Whole inner medulla of PTH treated rats (PTH, +, □, n=7) and control rats (control, -, ■, n=7) were processed for immunoblotting probed with antibodies recognizing proteins involved in actin cytoskeletal organization including cortactin (Cttn), ezirin-radixin-moesin (Erm), and non-muscle myosin IIb (Myh10). Densitometric analysis revealed that abundances of Cttn, and Erm were significantly down-regulated PTH-treated rats compared with control rats (P<0.05). The abundance of Myh10 was not changed in response to hypercalcemia.

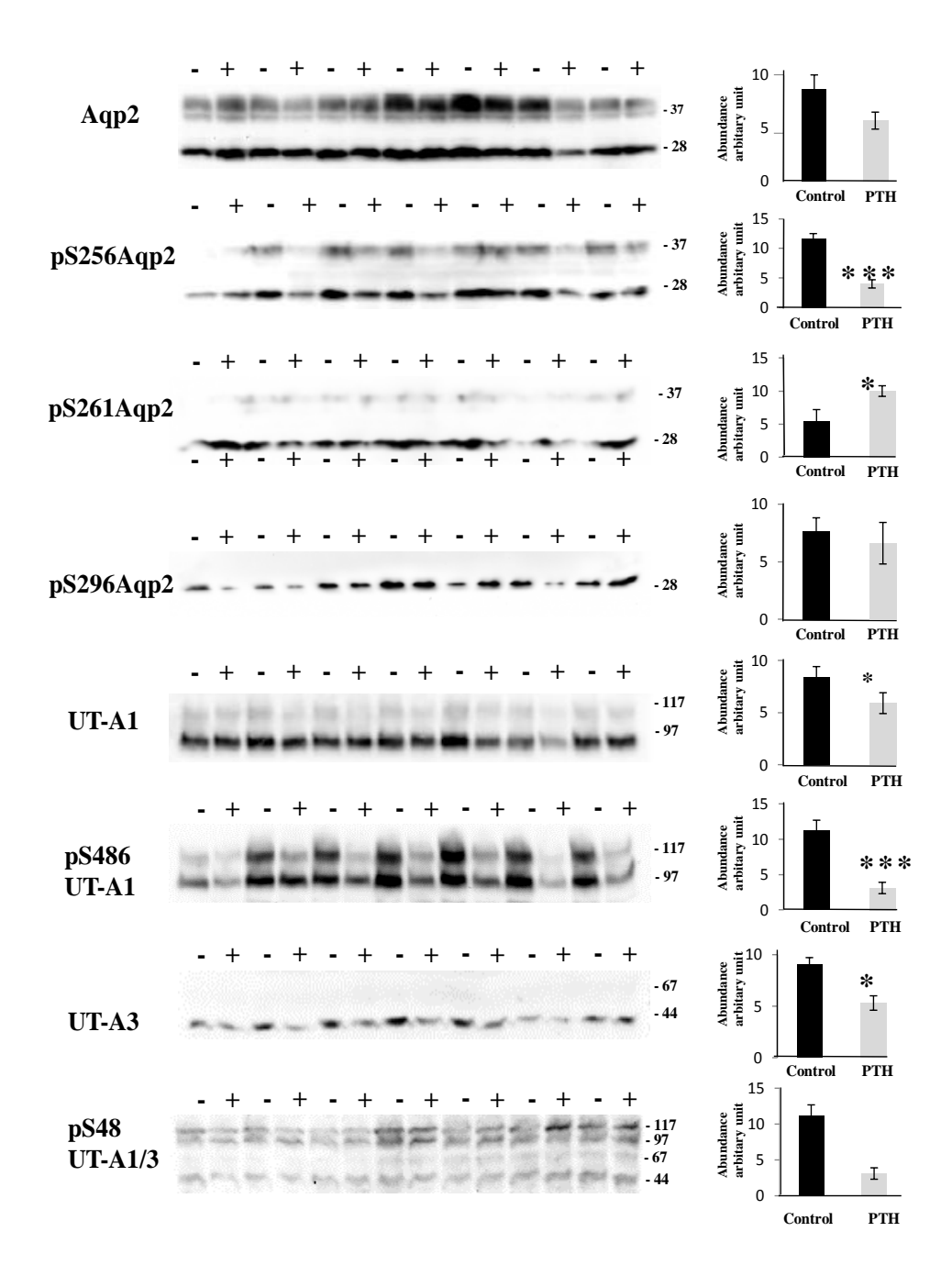


Figure 18. Immunoblotting of whole inner medulla of PTH treated rats (PTH, +, □, n=7) and control rats (control, -, ■, n=7) with Aqp2 antibody, phospho-specific Aqp2 antibodies, UT antibodies and phospho-specific UT antibodies. Densitometric analysis revealed unchanged total Aqp2 abundance and significantly down-regulation of phosphorylation at S256 Aqp2 by 65.5% (*** P<0.005) and significant up-regulation of pS261 Aqp2 by 81% (*P<0.05) in PTH-treated rats compared with control rats. The Aqp2 phosphorylation at S269 was not

changed in response to hypercalcemia. The abundances of total UT-A1, UT-A3 and phosphorylation at S486 of UT-A1 were significantly down-regulated in PTH-treated rats by 30% (*, P<0.05), 40% (*, P<0.05), and 72.3% (***, P<0.005), respectively. The phosphorylation at S84 of UT-A1/3 was not changed in response to hypercalcemia.

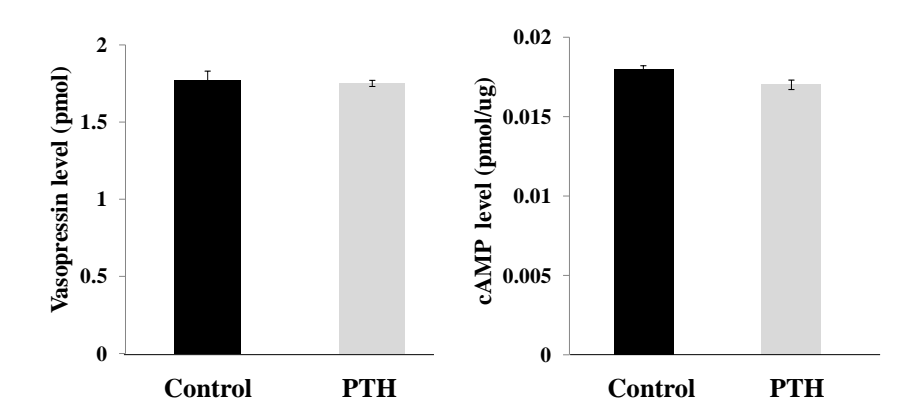


Figure 19. Serum vasopressin and whole inner medulla cAMP levels of PTH treated rats (PTH, □, n=7) and control rats treated with vehicle (Control, ■, n=7). (A) Serum vasopressin levels were not significantly different between PTH rats and control rats. (B) Whole inner medulla cAMP levels were not significantly different between PTH and control rats.

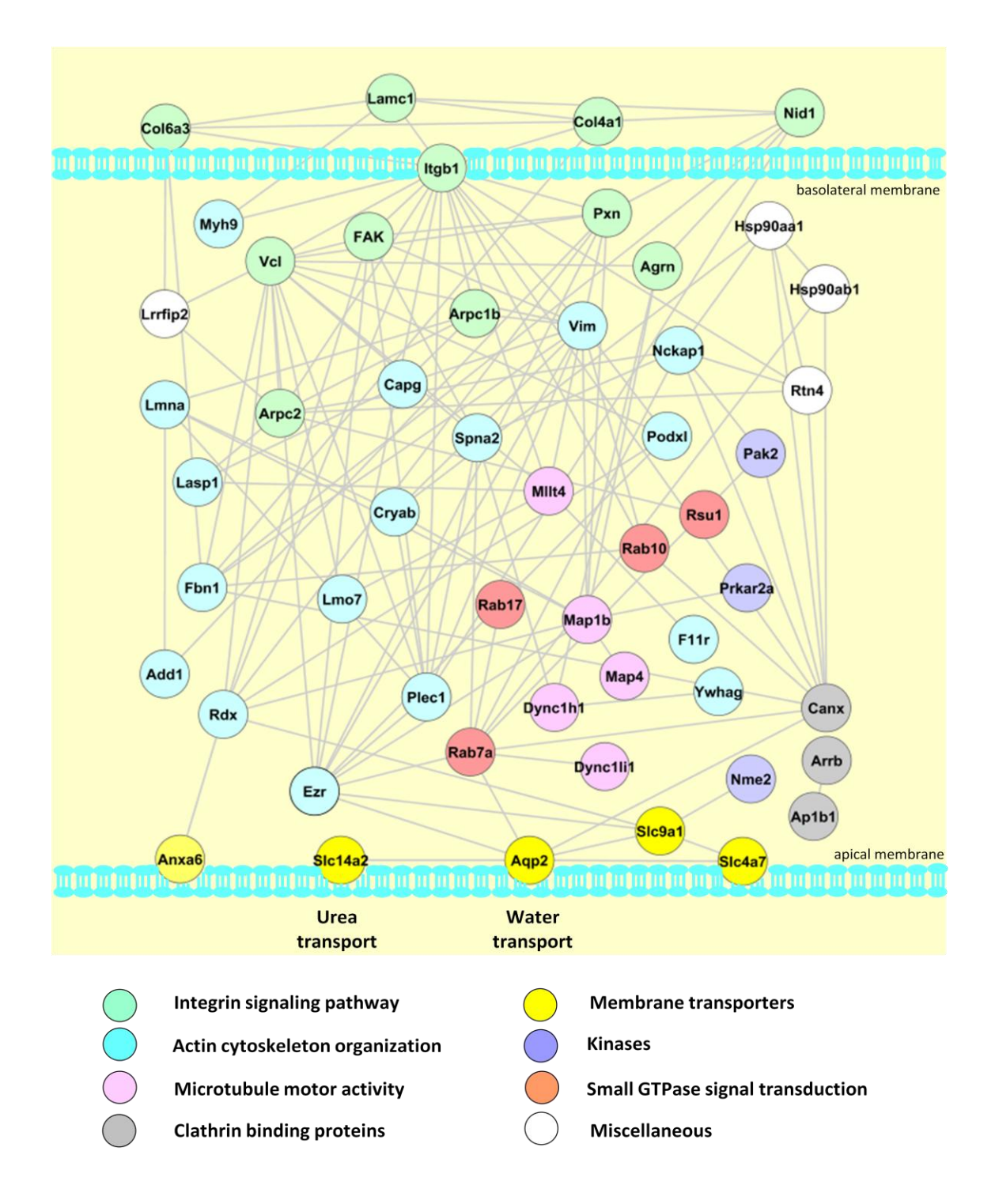
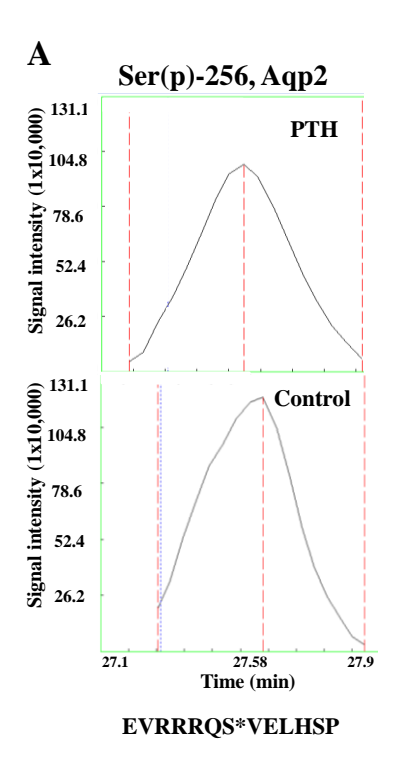
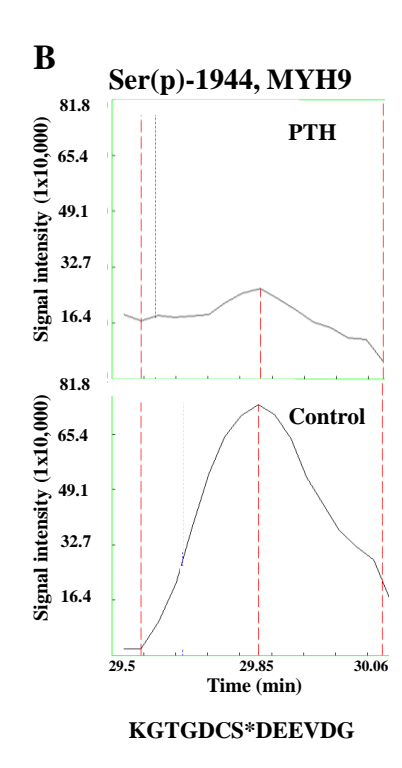


Figure 20. A signaling network in IMCD in response to hypercalcemia. Selected proteins and phosphoproteins that significantly changing in response to hypercalcemia were included in this figure. The network was formatted using String database (www.string_db.org).





Supplement Figure 1. MS quantitation of phosphopeptides is illulstrated by reconstructed peptide ion chromatograms from Qouil software. The data show the decreases in peak areas with PTH treatment compared with controls for (A) Phosphorylation of Aqp2 at S256 and (B) Phosphorylation of Myh9 at S1944

Acknowledgement

Funding support was from a Research Scholar Grant (RMU 5380032), The Thailand Research Fund and from Pediatric Nephrology Research Unit, Thammasat University.

Conflict of interest: All authors declared there is no conflict of interest.

Quantitative phosphoproteomics of hypercalcemia induced nephrogenic diabetes insipidus

S. Khositseth ¹, P. Somparn ¹, N. Thippamom ¹, P. Uawithya ², S-H Chen ³

¹Department of Pediatrics, Faculty of Medicine, Thammasat University, ²Department of Physiology, Faculty of Medicine, Siriraj Hospital, Mahidol University, Thailand, ³Department of Chemistry, National Cheng Kung University, Taiwan.

Nephrogenic diabetes insipidus (NDI) can cause by hypercalcemia (HC). The mechanism of NDI in parathyroid hormone induced HC was studied by using phosphoproteomic technique. Rats were infused with 30 µg/kg/day of PTH or vehicle for 1 day. Inner medulla collecting ducts from HC rats and control (C) were isolated. Tryptic phosphopeptides (immobilized metal affinity chromatography-enriched) were identified and quantified by mass spectrometry (LTQ-Orbitrap) using label free methodology. Phosphopeptide ratios were calibrated by total protein levels. Sixty nine and 180 phosphorylation sites were increased and decreased in HC, respectively. Significant down-regulation of phosphorylated forms of cytoskeletal proteins (Sept9, Sept2, Myh9, Myh10, Capg, Sptan1), β-catenin binding proteins (PXN, Ctnna1, LRRFlp1), and transmembrane transporters (Add1, Uso, Lrba) were revealed. Down-regulation of aquaporin-2(Aqp2) phosphorylation at S256 (by 60%), and S261 (by 50%), and decreased urea transporter (Slc14a2) phosphorylation at S62, and S63 (by 80%) were observed in HC. Immunoblots demonstrated 34% decrease of total Agp2 (P=0.08), 60% decrease of pS256 (P<0.001), 181% increase of pS261 (P<0.05), 30% decrease of total Slc14a2 (UT-A1) (P<0.05), 72% decrease of pS486, 41% decrease of total UT-A3 in the HC compared to the C, while pS84 was not changed. In conclusion, for the first time, important signaling molecules involved in urine concentration mechanism were identified in cellular mechanism of HC induced NDI. Two key proteins in urine concentrating mechanism, Aqp2 and Slc14a2, were found significantly decreased in both phosphorylated forms in HC induced NDI model in rat.

Quantitative phosphoproteomics of bilateral ureteral obstruction induced

nephrogenic diabetes insipidus

Sookkasem Khositseth¹, Panapat Uawithya², Poorichaya Somparn³,

¹Department of Pediatric, Faculty of Medicine, Thammasat University, ²Department of Physiology, Faculty of Medicine, Siriraj Hospital, Mahidol University, ³Biomedical Science, Graduate School, Chulalongkorn University.

Introduction. Obstructive uropathy is a common complication in adult and a common congenital urinary tract disease in children. Postobstructive diuresis or nephrogenic diabetes insipidus (NDI) commonly occurs after surgical treatment.

Objective. To study phosphoproteomic profiling in collecting duct in bilateral ureteral obstruction (BUO) induced NDI.

Materials and Methods. Quantitative phosphoproteomic analysis of inner medulla collecting ducts (IMCD) isolated from rat model of 12-h BUO was performed. The authors employed a combination of phosphopeptide enrichment by immobilized metal affinity chromatography and phosphorylation site identification by liquid chromatography-mass spectrometry (LC-MS/MS).

Results. In BUO rat model, down-regulations of AQP2 phosphorylation at S256, S261, S264, and Urea transporter phosphorylation at S62, S63, S67, S697 were identified by LC-MS/MS. The immunoblot of total AQP2 demonstrated decreased total AQP2 in BUO 0.2 times of control. The ratio of pS256/Total AQP2 in BUO was lower than those of controls (0.009 *vs.* 0.64). The immunoblot of UTA1/2 total protein decreased in BUO 0.25 times of control. The 11 and 16 phosphoproteins increased and decreased, respectively. The increased phosphoproteins involved in cytoskeletal reorganization (lima1, Plec, Pxn, Twf1, Sept2), vesicle trafficking (Ebag9), and transcriptional regulation (Ebag9, Eif4b), nucleotide binding protein (Hnrnpk, Pds5b, Rbm39, Top2a). The decreased phosphoproteins involved in cytoskeletal protein (Add1, Cnn3, Ctnna1, Ctnna2, Cttn, Myh9), nucleotide binding proteins (Hdgf, Hnrnpc, Hnrpd, Nucks1, Psip1), small G protein (Fgd2), and steroid binding protein (Pgrmc2).

Conclusion. BUO induced NDI due to down-regulation of aquaporin2, urea transporter protein and protein phosphorylation. Numbers of phosphoproteins in cytoskeletal regulation, transcription regulation, and vesicular trafficking were identified.

Quantitative proteomics of hypokalemia induced

nephrogenic diabetes insipidus

S. Khositseth^{1*}, P. Somparn², P. Uawithya³, S-H Chen⁴

¹Dept of Pediatrics, Thammasat Univ, ²Chulalongkorn Univ, ³Siriraj Hospital, Thailand, ⁴Natl Cheng Kung Univ, Taiwan.

Nephrogenic diabetes insipidus (NDI) can be caused by hypokalemia. The effect of early onset NDI due to hypokalemia was studied using proteomics profiling of rat kidney medullary collecting duct (IMCD). Rats were fed with potassium-free or regular diet. IMCDs were isolated on day1, protein extracts were subjected to in-gel trypsin digestion and analysis by label-free quantitative mass spectrometry. A total of 2,477 peptides corresponding to 821 proteins were identified, among which 189 proteins had significant change in abundance. Gene Ontology analysis revealed that hypokalemia significantly down-regulated proteins from adherens junction (Iqgap1, Rhoa, Vcl, Actn4, Ctnnd1, Ctnnb1), tight junction (Gbai1, Actn4, Myh10, Sptan1, Ctnnb1) and actin cytoskeletal organization (Itgb1, Cfl1, Vcl, Myh10, Ezr) (P<0.05). Immunoblotting demonstrated a 30% decrease of β-catenin (P<0.05), 23% decrease of total Aqp2 (P<0.05), 60% decrease of pS256-Aqp2 (P<0.001), 36.4 % decrease of pS261-Aqp2 (P<0.05), unchanged of total Slc14a2, and pS486-UTA1 abundances. In conclusion, this is the first report of the involvement of adherens junction, tight junction and actin cytoskeletal organization in hypokalemia-induced early onset NDI. Phosphopeptides of Aqp2 known to play important roles in urine concentrating mechanism were changed in abundance in hypokalemiainduced NDI.

Proteomics and Phosphoproteomics Profiling Reveal Involvement of Intergrin Signaling Pathway and Actin Cytoskeletal Organization in Hypercalcemia-induced

Nephrogenic Diabetes Insipidus

Sookkasem Khositseth^{1*}, Poorichaya Somparn², Panapat Uawithya³, Nattakan Thippamom¹, Atchara Paemanee⁴, Sittiruk Roytrakul⁴, Shu-Hui Chen⁵

¹Department of Pediatrics, Faculty of Medicine, Thammasat University, ² Faculty of Medicine, Chulalongkorn University, ³Department of Physiology, Faculty of Medicine, Siriraj Hospital, Mahidol University, ⁴National center for Genetic Engineering and Biotechnology, Thailand, ⁵Department of Chemistry, National Cheng Kung University, Taiwan.

Nephrogenic diabetes insipidus (NDI) can be caused by hypercalcemia. The effect of early onset NDI in parathyroid hormone (PTH)-induced hypercalcemia was studied using proteomics and phosphoproteomics profiling of rat kidney medulllary collecting duct (IMCD). Tryptic peptides and phosphopeptides were identified and quantified by mass spectrometry using a label-free methodology. A total of 5,866 peptides corresponding to 1,107 proteins and 1,388 phosphopeptides of 580 proteins were identified, with significant changes in abundance of 69 proteins and 49 phosphopeptides in early onset NDI. Gene Ontology terms and pathway analysis revealed that hypercalcemia-affected proteins and phosphoproteins are from integrin signaling pathway and actin cytoskeleton organization. Immunoblotting revealed altered abundances of vasopressin-regulated phosphorylation of aquaporin-2 (Aqp2) at Ser256 and Ser261, and decreased abundance of urea transporter UT-A1 (Slc14a2) and UT-A3, together with their phosphorylation at Ser486. This is the first report of the involvement of integrin signaling pathway in urine concentration mechanism in hypercalcemia-induced early onset NDI.

Proteomics Profiling Reveal Involvement of Adherens Junctions and Actin Cytoskeletal Organization in Hypokalemia-induced Nephrogenic

Diabetes Insipidus

S. Khositseth^{1*}, P. Somparn², P. Uawithya³, S-H Chen⁴

¹Dept of Pediatrics, Thammasat Univ, ²Chulalongkorn Univ, ³Siriraj Hospital, Thailand, ⁴Natl Cheng Kung Univ, Taiwan.

Nephrogenic diabetes insipidus (NDI) can be caused by hypokalemia. The effect of early onset NDI due to hypokalemia was studied using proteomics profiling of rat kidney medullary collecting duct (IMCD). Rats were fed with potassium-free or regular diet. IMCDs were isolated on day1, protein extracts were subjected to in-gel trypsin digestion and analysis by label-free quantitative mass spectrometry. A total of 2,477 peptides corresponding to 821 proteins were identified, among which 189 proteins had significant change in abundance. Gene Ontology analysis revealed that hypokalemia significantly down-regulated proteins from adherens junction (Iqgap1, Rhoa, Vcl, Actn4, Ctnnd1, Ctnnb1), tight junction (Gbai1, Actn4, Myh10, Sptan1, Ctnnb1) and actin cytoskeletal organization (Itgb1, Cfl1, Vcl, Myh10, Ezr) (P<0.05). Immunoblotting demonstrated a 30% decrease of β-catenin (P<0.05), 23% decrease of total Aqp2 (P<0.05), 60% decrease of pS256-Aqp2 (P<0.001), 36.4 % decrease of pS261-Aqp2 (P<0.05), unchanged of total Slc14a2, and pS486-UTA1 abundances. In conclusion, this is the first report of the involvement of adherens junction, tight junction and actin cytoskeletal organization in hypokalemia-induced early onset NDI. Phosphopeptides of Aqp2 known to play important roles in urine concentrating mechanism were changed in abundance in hypokalemiainduced NDI.